SUPPLEMENTARY INFORMATION

SUPPLEMENTARY METHODS

Ethics statement. All mouse and quail experiments were performed in strict accordance with all provisions of the Animal Welfare Act, the Guide for the Care and Use of Laboratory Animals, and the PHS Policy on Humane Care and Use of Laboratory Animals. The protocol was approved by the Institutional Animal Care and Use Committee (IACUC) of Wadsworth Center, New York State Department of Health (Protocol docket number 19-451). All efforts were made to minimize animal suffering.

Mice, quail, ticks, bacterial strains, human blood, animal sera, OmCI, and FH. BALB/c and Swiss Webster mice were purchased from Taconic (Hudson, NY). $C3^{-/-}$ mice in the BALB/c background were generated from the $C3^{-/-}$(C57BL/6) from Jackson Laboratory (Bar Harbor, ME) as described (1). *Coturnix* quail were purchased from Cavendish Game Birds Farm (Springfield, VT). *Ixodes scapularis* tick larvae were purchased from National Tick Research and Education Center, Oklahoma State University (Stillwater, OK) or obtained from the CDC through BEI Resources (Manassas, VA).

The *Escherichia coli, Pichia pastoris* and *Borrelia* strains used in this study are described in **Table S7**. *E. coli* strains DH5α, BL21(DE3), and derivatives were grown in LB broth or agar, supplemented with kanamycin (50µg/ml), ampicillin (100µg/ml), or no antibiotics as appropriate. *P. pastoris* strain X-33 was grown on YPD plates supplemented with zeocin (800µg/ml) or BMGY medium supplemented with 1% methanol. All *B. burgdorferi* strains were grown in BSK-II

completed medium supplemented with kanamycin (200µg/mL), streptomycin (50µg/mL), or no antibiotics (**Table S7**).

Mouse FH was purchased from MyBiosource (San Diego, CA). Quail FH and recombinant OmCI proteins were generated as described previously (1-4). The deidentified Human blood was obtained from BioIVT (BioIVT, Westbury, NY). The mouse and quail seha were obtained from Southern Biotech, Inc (Birmingham, AL) and Canola Live Poultry Market (Brooklyn, NY), respectively. The sera from white-footed mice were obtained previously (5). Prior to being used, all these sera were screened for antibodies against the C6 peptide of the *B. burgdorferi* protein VlsE (6) with the C6 Lyme ELISA kit (Diamedix, Miami Lakes, FL) to ensure the mice did not have prior exposure to *B. burgdorferi*.

Generation of recombinant CspZ proteins and recombinant human FH SCR6-7. To generate recombinant CspZ proteins for crystallization, $cspZ_{B379}$ (GenBank: FJ911671.1) and $cspZ_{B408}$ (GenBank: FJ911677.1) were amplified by PCR from the genomic DNA of *B. burgdorferi* strain B379 and B408 using the primers listed in **Table S8**. Note that B408 has two copies of *cspZ*, but they are functionally identical with only a single synonymous SNP at nucleotide 699 (4, 7). Based on the prediction by SignalP 4.1 (8) and according to our previous structural data from $CspZ_{B31}$ (9), the lipoprotein signal peptide (residues 1-22) was excluded from the amplified gene. The introduced *NcoI* and *NotI* restriction sites were used for ligation of the amplified fragments into the pETm-11 expression vector which contains the coding region for an N-terminal 6xHis tag and a tobacco etch virus (TEV) protease cleavage site. Expression in *E. coli*, purification by affinity chromatography, and 6xHis tag cleavage by TEV protease of both proteins $CspZ_{B379}$ and $CspZ_{B408}$

were performed similarly as described previously for $CspZ_{B31}$ (9). The purified and cleaved proteins were buffer exchanged into 10 mM Tris-HCl (pH 8.0) and concentrated to 11mg/ml using an Amicon centrifugal filter unit (Millipore, Burlington, MA, USA).

To produce recombinant human FH for crystallization, the gene encoding the SCR6-7 of human FH was synthesized by BioCat GmbH (Heidelberg, Germany) and cloned into pPICZαA vector behind the α-factor secretion signal using *XhoI* and *NotI* restriction sites in a way to restore the Kex2 signal cleavage site. The plasmid was linearized with *PmeI* and transformed by electroporation into *Pichia pastoris* (reassigned as *Komagataella phaffii*) strain X-33. Transformants were obtained on YPD agar plates containing 800µg/ml of the antibiotic zeocin. The selected clone was cultivated 24-h in BMGY medium at 30°C with aeration (250rpm) following addition of 1% methanol daily, and cultivation was continued for three more days. The cell pellet was removed by low-speed centrifugation. Supernatant was buffer-exchanged into 50mM sodium phosphate (pH 6.0) by Sephadex G-25 Fine column (bed volume 360ml) (Cytiva, Marlborough, MA, USA) in 100ml portions at a flow rate of 20ml/min. Two liters of supernatant was passed through the CaptoS Improved Resolution column (bed volume 20ml) (Cytiva, Marlborough, MA, USA) and bound material was eluted with a linear salt gradient at a flow rate of 6ml/min. Target protein fractions were selected based on SDS-PAGE. The relevant fractions were pooled and buffer-exchanged into 20mM Tris-HCl (8.0), 50mM NaCl and 10mM NaH_2PO_4 using an Amicon filter device (Millipore, Burlington, MA, USA).

To generate recombinant $CspZ_{B379}$ and $CspZ_{B408}$ for the studies other than crystallization, the region encoding $cspZ_{B379}$ or $cspZ_{B408}$ without the signal peptide was amplified as described above and engineered to encode *BamHI* and *SalI* sites at the 5’ and 3’ ends, respectively, allowing

subsequent cloning into the pJET cloning vector (Thermo Fisher Scientific, Waltham, MA). These pJET-derived plasmids encoding $cspZ_{B379}$ or $cspZ_{B408}$ were used as template for site-directed, ligase-independent mutagenesis (SLIM) (**Table S7, S8**) to generate plasmids producing $CspZ_{B379}$-L_{B408} and $CspZ_{B408}$-L_{B379} (10). After verifying the sequences of all the plasmids (Wadsworth ATGC facility), the DNA fragments were subsequently excised using *BamHI* and *SalI* and then inserted into the same sites in pGEX4T2 (GE Healthcare, Piscataway, NJ) (2). The pGEX4T2-derived plasmids were then transformed into the *E. coli* strain BL21(DE3). The GST-tagged CspZ proteins were produced and purified by affinity chromatography. These proteins were verified for their secondary structures not impacted by the mutagenesis using CD (**Fig. S16**), as described in the section "Circular dichroism (CD) spectroscopy."

To generate recombinant CspZ from the last common ancestor states, pET-28a+ encoding these states flanked by *BamHI* and *SalI* sites at the 5' and 3' ends, respectively, were cloned (Synbio Technologies, Monmouth Junction, NJ). The plasmids were transformed into the *E. coli* strain BL21(DE3), and the His-tagged CspZ proteins were produced and purified by affinity chromatography.

Crystallization and structure determination. For crystallization of $CspZ_{B379}$ and $CspZ_{B408}$, 96-well sitting drop plates were set using a Tecan Freedom EVO100 workstation (Tecan Group, Männedorf, Switzerland) by mixing 0.4µl of protein with 0.4µl of precipitant using the 96-reagent sparse-matrix screens JCSG+ and Structure Screen 1&2 (Molecular Dimensions, Newmarket, UK). The crystals for $CspZ_{B379}$ were obtained in 0.2M Ammonium citrate and 24% PEG 3350. For $CspZ_{B408}$, the crystals were formed in 0.2M potassium acetate, 0.1M Tris-HCl (pH 8.0) and 28%

PEG 3350. Prior to the data collection, the crystals were frozen in liquid nitrogen. An additional 20% glycerol was used as a cryoprotectant for $CspZ_{B379}$ crystals, whereas the respective precipitant with an additional 14% glycerol was used as cryoprotectant for $CspZ_{B408}$ crystals.

$CspZ_{B408}$ (4mg/ml) and human SCR6-7 (3mg/ml) were mixed together at a molar ratio of 1:2 and loaded on a HiLoad 16/600 Superdex 200 prep grade column (GE Healthcare, Chicago, IL, USA) pre-equilibrated with 20mM Tris-HCl (8.0), 50mM NaCl and 10mM NaH_2PO_4. The flow rate was set to 2ml/min. Size exclusion chromatography resulted in one major peak containing the complex, confirmed by SDS-PAGE. Crystallization was set as described earlier for $CspZ_{B379}$ and $CspZ_{B408}$ by mixing 0.4µl of protein with 0.4µl of precipitant and using the 96-reagent sparse-matrix screens. The crystals for $CspZ_{B408}$-SCR6-7 complex were obtained in 0.2M Zinc acetate, 0.1M imidazole (pH 7.4) and 10% PEG 3000. Crystals were frozen in liquid nitrogen by using 20% glycerol as a cryoprotectant.

Diffraction data for $CspZ_{B379}$, $CspZ_{B408}$ and $CspZ_{B408}$-SCR6-7 complex were collected at the MX beamline instrument BL 14.1 at Helmholtz-Zentrum, Berlin (11). Reflections were indexed by XDS and scaled by AIMLESS from the CCP4 suite (12-14). Initial phases for $CspZ_{B379}$ and $CspZ_{B408}$ were obtained by molecular replacement using Phaser (15), with the crystal structure of the orthologous protein $CspZ_{B31}$ was used as a searching model (97% sequence identity, PDB: 4CBE). For $CspZ_{B408}$-SCR6-7 complex, the phases were determined using $CspZ_{B408}$ (PDB: 7ZJK, RMSD: 0.98 Å) and human FH SCR6-7 (PDB: 4AYD-A, RMSD: 0.98 Å) as the searching models. After molecular replacement, the protein models were built automatically in BUCCANEER (16). The crystal structures were improved by manual rebuilding in COOT (17). Crystallographic refinement was performed using REFMAC5 (18). A summary of the data collection, refinement

and validation statistics for $CspZ_{B379}$, $CspZ_{B408}$ and $CspZ_{B408}$-SCR6-7 complex are given in **Table S9.**

Protein 3D structure prediction using AlphaFold. AlphaFold v2.0 (19) was used to predict the 3D structure for quail FH SCR6-7 extrapolated from the sequences of *Coturnix japonica* FH (GenBank: XM_015869474.2). Structure prediction with AlphaFold v2.0 was performed at default parameters (https://github.com/deepmind/alphafold/) running on AMD Ryzen Threadripper 2990WX 32-Core; 128 GB RAM; 4 x NVIDIA GeForce RTX 2080, and using the full databases downloaded on 2021-09-25. For further structural analysis, only the predicted structure with the highest confidence was used (as ranked by using LDDT (pLDDT) scores).

Circular dichroism (CD) spectroscopy. CD analysis was performed on a Jasco 810 spectropolarimeter (Jasco Analytical Instrument, Easton, MD) under nitrogen. CD spectra were measured at room temperature (RT, 25°C) in a 1mm path length quartz cell. Spectra of each of the CspZ proteins (10μM) were recorded in phosphate based saline buffer (PBS) at RT, and three far-UV CD spectra were recorded from 190-250nm in 1nm increments for far-UV CD. The background spectrum of PBS without proteins was subtracted from the protein spectra. CD spectra were initially analyzed by the software Spectra Manager Program (Jasco). Analysis of spectra to extrapolate secondary structures were performed using the K2D3 analysis programs (20).

ELISAs. Quantitative ELISA was used to determine FH-binding by CspZ proteins, or ancestral proteins, as described previously (1, 21), with the following modifications: Mouse anti-GST tag

or mouse anti-His tag 1:200× (Sigma-Aldrich) and HRP-conjugated goat anti-mouse IgG 1:2,000× (Seracare Life Sciences) were used as primary and secondary antibodies, respectively, to detect the binding of GST- or histidine-tagged proteins.

Surface Plasmon Resonance (SPR). Interactions of CspZ proteins with FH were analyzed by SPR using a Biacore T200 (Cytiva, Marlborough, MA). Ten micrograms of mouse or quail FH were conjugated to a CM5 chip (Cytiva) as described previously (21). For quantitative SPR experiments, 10µL of increasing concentrations (0.08, 0.03125, 0.0125, 0.5, 2µM) of each of the CspZ proteins were injected into the control cell and the flow cell immobilized with FH at 10µl/min, 25^{o}C. To obtain the kinetic parameters of the interaction, sensogram data were fitted by means of BIAevaluation software version 3.0 (GE Healthcare), using the one step biomolecular association reaction model (1:1 Langmuir model), resulting in optimum mathematical fit with the lowest Chi-square values.

Shuttle vector construction and plasmid transformation into *B. burgdorferi*. "Loop swapped" CspZ variants (i.e., $CspZ_{B379}L_{B408}$ and $CspZ_{B408}L_{B379}$) were designed based on the full-length sequences (B379 accession: OM643341; B408: accession: OM643340) and purchased as double-stranded DNA fragments flanked by *BamHI* and *SalI* on the 5' and 3', respectively (Integrated DNA Technologies, Inc., Coralville, IA). B31-A3Δ*cspZ* was complemented with these variants, or with native CspZ from B379 and B408 flanked by the same restriction enzyme sites (**Table S7**), in the same manner as the previously published strains of B31-A3Δ*cspZ*/pKFSS and B31-A3Δ*cspZ*/p$CspZ_{B31}$ (2).

154 The plasmid profiles of these spirochetes were examined to ascertain identical profiles
155 between these strains and their parental strain B31-A3 (22). The generation time of these
156 transformants was calculated as previously described (2). We also verified the strains were not
157 affected by dosage effect, which can be caused by significant differences between the copy
158 numbers of the native and complemented locations: herein, *Bb* plasmid lp28-3 and the shuttle
159 vector pKFSS-1, respectively. We obtained the number of copies for a gene on shuttle vector
160 pKFSS (*colE1*) or lp28-3 (*bbh17*) by performing qPCR using the primers listed in **Table S8** (23,
161 24). The details on qPCR herein are outlined in the section, "Quantification of Spirochete Burden".
162 These samples included the DNA extracted from *in vitro* cultivated complemented Δ*cspZ* strains,
163 or the hearts from the mice and quail infected with each of these strains at 10dpf. The ratio of copy
164 numbers between pKFSS vs. lp28-3 from each strain was close to one, suggesting any observed
165 phenotypes of these strains are unlikely resulting from dosage effects (**Table S10**).
166
167 **Flow cytometry.** CspZ production and FH-binding on spirochete surface were determined as
168 described (1), including blood-treatment to induce the production of CspZ (2). To determine the
169 levels of mouse C5b-9 or quail C8 deposition on the surface of spirochetes, mouse or quail sera
170 were incubated with $1x10^7$ spirochetes in PBS at a final concentration of 20% at 25°C for one hour.
171 After incubation, spirochetes were washed then resuspended in HBSC-DB (25mM Hepes acid,
172 150mM sodium chloride, 1mM $MnCl_2$, 1mM $MgCl_2$, 0.25mM $CaCl_2$, 0.1% glucose, and 0.2%
173 BSA). Rabbit anti-mouse C5b-9 polyclonal IgG (1:250x) (Complement Technology, Tyler, TX)
174 or mouse anti-quail C8 polyclonal sera (1:250x) (4) were used as the primary antibodies. An Alexa
175 647-conjugated goat anti-rabbit (ThermoFisher) or a goat anti-mouse IgG (ThermoFisher) (1:250x)

was used as the secondary antibody. After staining, the spirochetes were fixed with 0.1% formalin. The resulting fluorescence intensity of spirochetes was measured and analyzed by flow cytometry using a FACSCalibur (BD Bioscience) as described (2, 4).

Serum resistance assays. The serum resistance of *B. burgdorferi* was measured as described with modifications (1, 2, 5). Cultures in mid-log phase of each strain treated with human blood (2), as well as the high passaged, non-infectious, and serum-sensitive human blood-treated *B. burgdorferi* strain B313 (control), were cultivated in triplicate and diluted to a final concentration of 5×10^6 cells/mL in 100µl of BSK-II medium without rabbit sera. The cell suspensions were mixed with sera collected from naïve white-footed mice or quail (60% spirochetes and 40% sera) in the presence or absence of 2µM of CVF (Complement Technology) or recombinant OmCI, to deplete complement from mouse and quail sera, respectively. Heat-inactivated sera (65°C for 2-h) were also included in assays assessing OmCI functionality at 11 days post inoculation (dpi).

Bacterial survivability was determined by microscopically counting the number of live bacteria after live/dead staining or by measuring the number of colonies forming units (CFUs) after plating the sera-spirochete mixtures on agar plates. To determine the number of live bacteria using live/dead staining, spirochetes incubated with sera at 0- and 4-h were mixed with 1× SYBR Green I (ThermoFisher) and 6µM of propidium iodide (ThermoFisher) in 0.5% BSA in PBS as described (2, 3, 25). We visualized the live (green) and dead (red) spirochetes using the FITC and Texas Red filters from an Olympus BX51 fluorescence microscope (Olympus Corporation, Waltham, MA). To determine the CFUs, aliquots of the sera-spirochete mixtures at 0- and 4-h post incubation were mixed with 1.8% agarose (BioRad; Hercules, CA), followed by plating on a

198 solidified BSK II/agarose layer in sterilized 100 x 20mm tissue culture dishes (Corning
199 Incorporated, Corning, NY), as described previously (26, 27). Plates were incubated at 33ºC in 5%
200 CO_2 for two weeks. The percent survival of *Bb* was calculated by the normalization of the number
201 of live spirochetes or CFUs at 4-h post incubation, to those immediately after incubation with sera
202 (0-h). We determined the percent survival of the WT B31-A3 and Δ*cspZ*/Vector incubated with
203 white-footed mouse or quail sera using each of three methodologies. As the results obtained from
204 these methodologies were comparable (**Fig. S7)**, (3), the rest of the serum resistance assays were
205 performed using live/dead staining.
206
207 **Mouse and quail infection by ticks.** Generating flat, infected *I. scapularis* nymphs has been
208 described previously (1, 28). The infected nymphs were placed in a chamber to feed on 4- to 6-
209 week-old male and female BALB/c or $C3^{-/-}$ mice in BALB/c background, or on four- to six-week-
210 old male and female untreated or OmCI-treated quail, as described previously (29). For OmCI-
211 treatment, the quail were subcutaneously injected with OmCI (1mg/kg of quail) one day prior to
212 the nymph feeding. Every group had five animals/group, with the following exceptions: (1)
213 BALB/c blood from the B31-A3 and Δ*cspZ*/Vector groups at 10dpf (**Figs 3F, S10G**), which
214 included data from initial trial experimentations and totaled six or nine mice per group,
215 respectively; (2) all tissues from quail infected with Δ*cspZ*/Vector at 9dpf (**Fig S10P-S)** to enhance
216 the rigor of the work.
217 The engorged nymphs were obtained from the chambers at four days post tick feeding.
218 Animals were sacrificed, and tissues were collected from the mice at 7-, 10-, or 14dpf (blood, tick
219 bite site of the skin, heart, bladder, tibiotarsus joint), and quail (blood, tick bite site of the skin,

heart, brain) at 9-, or 14dpf-. To ensure OmCI was still functional at these timepoints, quail were subcutaneously injected with OmCI (1mg/kg of quail) or PBS buffer (control), and the sera were collected at 10dpi (equivalent to 11dpf). The lack of the ability of this serum to kill the sera-sensitive *B. burgdorferi* strain B313 (i.e., to ensure complement was still depleted) was assessed as described in the section "Serum resistance assays" (**Fig. S17**).

Quantification of spirochete burden. The DNA from tissues, blood, and ticks was extracted as described previously (29). qPCR was then performed to quantitate spirochete burden using an ABI 7500 Real-Time PCR System (ThermoFisher Scientific) in conjunction with PowerUp SYBR Green Master Mix (ThermoFisher Scientific). The amplification cycle of the Lyme borreliae *recA* gene using the primer listed in **Table S8**, as described (2). Although the ratio of the number of genomes (i.e., the copies of *recA*) to the number of spirochetes is not always equal to one, within the same life stages or environment, the number of genomes is correlated with the number of bacteria (30). Therefore, we established a standard curve using a known number of *in vitro* cultivated *B. burgdorferi* strain B31-A3 to the *recA*-derived threshold cycle (Cq) values. By applying the Cq values of *recA* derived from the experimental samples, we could extrapolate relative spirochete burdens in each sample. In a similar manner, we determined the number of copies of mouse nidogen and quail β-actin for the samples derived from mice and quail, respectively, using the primers listed in **Table S8**, as described (26, 28, 31, 32). We then normalized the spirochete burden (*recA* copies) to 10^4 copies of mouse nidogen or quail β-actin for each respective tissue type (**Fig. 3E to M, S10-11**).

Genomic and evolutionary analyses. To generate the *cspZ* phylogenetic trees, we mined all publicly available *cspZ* sequences on NCBI as of September 2021, including assembled genomes, nucleotides, and unassembled genomes on the SRA. To pull *cspZ* from unassembled genomes, the short reads were aligned to *cspZ* from B31, B379, or B408 with UGENE v39.0 using BWA-MEM at defaults (33, 34). Strains were removed from the analyses if the coverage was too low, there was evidence of PCR/sequencing errors (e.g., non-conserved homopolymer length) or multiple CspZ variants within one strain. All resulting 174 *cspZ* sequences, plus the outgroup strains (*B. spielmanii* A14s accession: EU272854.1; *B. afzelii* FEM4 accession: OM243915; *B. afzelii* VS461 accession: MN809989.1; *B. garinii* PBr accession: CP001307.1; *B. bissettii* DN127 accession: NC_015916.1; *B. bissettii* CO275 accession: JNBW01000464.1), were aligned by codons using TranslatorX (35). All isolates were collapsed into haplotypes in FaBox v1.61, and these haplotypes were used with the *B. bissettii* outgroup to generate a NeighborNet network in SplitsTree v4 (36, 37). Phylogenetic trees were estimated using likelihood as optimality criterion in IQ-tree v1.6.12 (38) and a full substitution model search procedure in ModelFinder (39). Internode branch support was estimated with 10,000 replicates of both ultrafast bootstrapping and the SH-aLRT branch test (38-40). All resulting phylogenetic trees were visualized in iTOL v6.4.3 (41). The pairwise sequence similarity for each of the 174 *B. burgdorferi cspZ* isolates relative to $CspZ_{B31}$, $CspZ_{B408}$, or $CspZ_{B379}$ was determined in MEGA-X with default settings (42). Putative recombination breakpoints were analyzed with GARD (43), and evidence of selection was determined using BUSTED (44, 45), FUBAR (46), FEL (47) and MEME (48), all on the Datamonkey server (49). The ancestor state for the entire *B. burgdorferi* ingroup was reconstructed using the LG model in GRASP 2020.05.05 (50, 51), as well as FireProt-ASR with default settings (52) using both full

and haplotype phylogenies, the multitaxon outgroup, and solely *B. bissettii* as the outgroup. Divergence dating was carried out in BEAST v1.10.4 (53) using the HKY+Γ_4 substitution model (54, 55), a coalescent Bayesian skyline coalescent model, and a strict clock with a uniform prior on the substitution rate using the previously determined rate of 4.75e-06 substitutions/site/year (56). A Markov chain Monte Carlo chain length of 100 million steps was used with a 10,000-step thinning, resulting in effective sample sizes greater than 200, an indication of an adequate chain mixing. The analyses were run in triplicate and combined after removing a 10% burn-in.

The amino acids encoding SCRs 6-7 from human (GenBank accession U56979.1), mouse (NM_009888.3), and quail (XM_015869474.2) FH, or $CspZ_{B31}$, $CspZ_{B379}$, $CspZ_{B408}$, the loop-swapped variants, and the reconstructed ancestral CspZ sequences were aligned in MEGA-X using ClustalW with default settings, analyzed with ESPript v3.0, and visualized with Jalview v2.11.0 (42, 57, 58).

Statistical analysis. Samples were compared using the Mann-Whitney *U* test or the Kruskal-Wallis test with the two-stage step-up method of Benjamini, Krieger, and Yekutieli (59).

Accession numbers. The coordinates and the structure factors for $CspZ_{B379}$, $CspZ_{B408}$, and human SCR-$CspZ_{B408}$ have been deposited in the Protein Data Bank with accession codes 7ZJJ, 7ZJK, and 7ZJM, respectively.

SUPPLEMENTAL TABLES

Table S1: $CspZ_{B408}$ residues that bind to human FH based on CspZB408-human SCR6-7 complex structure and their equivalent residues in $CspZ_{B31}$ and $CspZ_{B379}$.

$CspZ_{B408}$	$CspZ_{B31}$	$CspZ_{B379}$
Asp47	Asp47	Asp47
Tyr50	Tyr50	Tyr50
Asn51	Asn51	Ser51
Thr54	Thr54	Thr54
Asn58	Asn58	Asn58
Thr62	Thr62	Thr62
Asp71	-	-
Asp73[a]	Asp70[a]	Asp74[a]
Ser75[a]	Ser72[a]	Ser76[a]
Arg142	Arg139	Arg143
Asn183	Asn180	Asn184
Tyr214	Tyr211	Tyr215

[a]Interacts with SCR6.

Table S2. CspZ variants differ in binding to Factor H from different animals

		ELISA[a]	----- Surface Plasmon Resonance[b] -----		
CspZ variant	**Factor H source**	**K_D (µM)**	**K_D (µM)**	k_{on} ($10^3 s^{-1} M^{-1}$)	k_{off} (s^{-1})
$CspZ_{B31}$	**Mouse**	**0.43±0.74[c]**	**0.20±0.02**	45.78±15.36	0.0084±0.0022
	Quail	**0.91±0.08[d]**	**0.81±0.01**	117.43±3.25	0.095±0.0032
$CspZ_{B379}$	**Mouse**	**n.b.[d]**	**n.b.**	n.b.	n.b.
	Quail	**0.59±0.037**	**0.75±0.15**	119.83±7.08	0.088±0.012
$CspZ_{B379}L_{B408}$	**Mouse**	**1.39±0.12**	**0.90±0.12**	21.16±10.58	0.018±0.0094
	Quail	**n.b.**	**n.b.**	n.b.	n.b.
$CspZ_{B408}$	**Mouse**	**0.68±0.05**	**0.20±0.02**	22.13±1.31	0.008±0.002
	Quail	**n.b.**	**n.b.**	n.b.	n.b.
$CspZ_{B408}L_{B379}$	**Mouse**	**n.b.**	**n.b.**	n.b.	n.b.
	Quail	**1.38±0.47**	**0.99±0.06**	72.43±2.14	0.072±0.006
GST[e]	**Mouse**	**n.b.**	**n.d.**	n.d.	n.d.
	Quail	**n.b.**	**n.d.**	n.d.	n.d.

All values represent the mean ± SEM of three experiments

[a]Determined using GST tagged CspZ variants or mutant proteins.

[b]Determined using untagged CspZ variants or mutant proteins

[c]Reported previously in (60)

[d]No binding activity was detected

[e]GST was included as a negative control

Table S3. The generation time for *B. burgdorferi* strains used in this study.

Strain	Generation time (h)[a, b]
B31-A3	16.45 ± 1.38
B31-A3Δ*cspZ*/vector	16.42 ± 1.79
B31-A3Δ*cspZ*/pCspZ$_{B31}$	17.12 ± 1.05
B31-A3Δ*cspZ*/pCspZ$_{B379}$	16.62 ± 2.07
B31-A3Δ*cspZ*/pCspZ$_{B379}$L$_{B408}$	16.40 ± 0.83
B31-A3Δ*cspZ*/pCspZ$_{B408}$	17.31 ± 0.62
B31-A3Δ*cspZ*/pCspZ$_{B408}$L$_{B379}$	18.66 ± 2.06

[a]The generation time was calculated as described previously (2).

[b]There were no significant differences between generation time of any strain (Kruskal-Wallis test with the two-stage step-up method of Benjamini, Krieger, and Yekutieli)

Table S4: The percentage of SAPs in CspZ variants

Loop type	Position	AA	%	AA	%
$CspZ_{B408}$	20	Asp	64.00	Asn	36.00
	30	Asp	88.00	Asn	36.00
	41	Val	56.00	Phe	44.00
	84	Phe	52.00	Leu	48.00
	95	Lys	92.00	Asn	8.00
	107	Met	56.00	Ile	44.00
	183	Asp	52.00	Asn	48.00
$CspZ_{B31}$	30	Asn	88.30	Asp	11.70
	66[a]	Gly	80.85	Val	19.15
	68[a]	Phe	80.85	Tyr	19.15
	81	Phe	88.30	Leu	11.70
	88	Val	98.94	Ala	1.06
	131	Val	94.68	Ala	5.32
	154	Ser	98.64	Pro	1.06
	161	Lys	96.81	Glu	3.19
	203	Ser	98.94	Lys	1.06
	204	Arg	98.94	Leu	1.06
	208	Asn	67.02	Asp	32.98
$CspZ_{B379}$	30	Asp	87.50	Asn	12.50
	50[b]	Tyr	97.92	His	2.08
	235	Ile	97.92	Ser	2.08

[a]Part of the loop structures

[b]Predicted to directly interact with FH

307 **Table S5. Estimated diversification times for each lineage**.

Lineage	Median[a]	HPD95%[a]
CspZ-B31	784	263-1860
CspZ-B379	261	59-741
CspZ-B408	671	179-1679

308 [a]Years before present

309

310 **Table S6**. **CspZ variants differ in binding to Factor H from different animals**

		ELISA[a]	**----- Surface Plasmon Resonance[b] -----**		
CspZ variant	**Factor H source**	**K_D (μM)**	**K_D (μM)**	k_{on} ($10^3 s^{-1} M^{-1}$)	k_{off} (s^{-1})
$CspZ_{B31}$	**Human**	**0.31±0.03**	**0.15±0.07**	27.13±8.10	0.0037±0.0010
	Mouse	**0.38±0.07**	**0.20±0.02**	45.78±15.36	0.0084±0.0022
	Quail	**0.74±0.15**	**0.81±0.01**	117.43±3.25	0.095±0.0032
$CspZ_{LCAS1}$	**Human**	**0.34±0.10**	**0.081±0.027**	22.73±2.81	0.0018±0.0005
	Mouse	**0.41±0.07**	**0.19±0.10**	20.76±2.98	0.0041±0.0028
	Quail	**0.77±0.09**	**0.91±0.17**	85.00±43.34	0.083±0.050
$CspZ_{LCAS2}$	**Human**	**0.23±0.02**	**0.058±0.02**	24.73±0.40	0.0014±0.0004
	Mouse	**0.36±0.05**	**0.21±0.03**	25.60±2.35	0.0055±0.0007
	Quail	**0.94±0.09**	**0.95±0.07**	122.50±11.87	0.091±0.063
$CspZ_{LCAS3}$	**Human**	**0.25±0.02**	**0.073±0.012**	27.56±2.28	0.0020±0.0003
	Mouse	**0.53±0.12**	**0.19±0.058**	27.36±0.28	0.0052±0.0012
	Quail	**0.73±0.06**	**0.75±0.28**	132.13±10.09	0.082±0.045
$CspZ_{LCAS4}$	**Human**	**0.30±0.01**	**0.13±0.01**	18.20±0.67	0.0022±0.0016
	Mouse	**0.40±0.01**	**0.11±0.014**	26.46±0.72	0.0029±0.0003
	Quail	**0.93±0.06**	**0.61±0.04**	306.0±1.25	0.16±0.01
DbpA[c]	**Human**	**n.b.[d]**	**n.d.[e]**	n.d.	n.d.
	Mouse	**n.b.**	**n.d.**	n.d.	n.d.
	Quail	**n.b.**	**n.d.**	n.d.	n.d.

311 All values represent the mean ± SEM of three experiments
312 [a]Determined using His tagged CspZ proteins shown in Fig. S14
313 [b]Determined using His tagged CspZ proteins shown in Fig. S14, except for the interactions of $CspZ_{B31}$ with mouse and quail FH
314 shown in Fig. 2A and Table S2
315 [c]His tagged DbpA as a negative control
316 [d]No binding activity was detected
317 [e]Not determined
318

Table S7. The strains and plasmids used in this study.

Strain or plasmid	Genotype or characteristic	Source
B. burgdorferi		
B313	High-passage *B. burgdorferi* B31 missing lp5, lp17, lp21, lp25, lp28-1, lp28-2, lp28-3, lp28-4, lp36, lp38, lp54, lp56, cp9, cp32-4, cp32-6, cp32-8, cp32-9	(61)
B31-A3	Clone of *B. burgdorferi* B31 missing cp9 RST type 1, *ospC* type A	(62)
B379	Clone of *B. burgdorferi* B379 isolated from humans with erythema migrans. RST Type 2, *ospC* type K	(21)
B408	Clone of *B. burgdorferi* B379 isolated from humans with erythema migrans. RST type 3, *ospC* type K	(21)
B31-A3Δ*cspZ*	B31-A3Δ*cspZ*::KanR[a]	(63)
B31-A3Δ*cspZ*/Vector	B31-A3Δ*cspZ*::KanR carrying plasmid pKFSS	(2)
B31-A3Δ*cspZ*/pCspZ$_{B31}$	B31-A3Δ*cspZ*::KanR complemented with intact *cspZ* driven by the promoter of *cspZ$_{B31}$*	(2)
B31-A3Δ*cspZ*/pCspZ$_{B379}$	B31-A3Δ*cspZ*::KanR complemented with intact *cspZ$_{B379}$* driven by the promoter of *cspZ$_{B31}$*	This study
B31-A3Δ*cspZ*/pCspZ$_{B408}$	B31-A3Δ*cspZ*::KanR complemented with intact *cspZ$_{B408}$* driven by the promoter of *cspZ$_{B31}$*	This study
B31-A3Δ*cspZ*/pCspZ$_{B379}$L$_{B408}$	B31-A3Δ*cspZ*::KanR complemented with intact *cspZ $_{B379}$* except the residues 190 to 216 replaced by residues 190 to 213 from *cspZ$_{B408}$* ,driven by the promoter of *cspZ$_{B31}$*	This study

B31-A3Δ*cspZ*/pCspZ$_{B408}$L$_{B379}$	B31-A3Δ*cspZ*::KanR complemented with intact *cspZ $_{B408}$* except the residues 190 to 213 replaced by residues 190 to 216 from *cspZ$_{B379}$*, driven by the promoter of *cspZ$_{B31}$*	This study
E. coli		
DH5α	F- Φ80lacZΔM15 Δ(lacZYA-argF) U169 recA1 endA1 hsdR17(rk-, mk+) phoA supE44 thi-1 gyrA96 relA1 λ-	ThermoFisher
BL21(DE3)	F−, ompT hsdSB (rB− mB−) gal dcm (DE3)	Novagen
BL21(DE3)/pGEX4T2-CspZ$_{B31}$	BL21(DE3) producing GST-tagged residues 58 to 711 of CspZ$_{B31}$	(2)
BL21(DE3)/pGEX4T2-CspZ$_{B379}$	BL21(DE3) producing GST-tagged residues 58 to 723 of CspZ$_{B379}$	This study
BL21(DE3)/pGEX4T2-CspZ$_{B408}$	BL21(DE3) producing GST-tagged residues 58 to 720 of CspZ$_{B408}$	This study
BL21(DE3)/pGEX4T2-CspZ$_{B379}$L$_{B408}$	BL21(DE3) producing GST-tagged residues 58 to 723 of CspZ$_{B379}$ except the residues 190 to 216 replaced by residues 190 to 213 from CspZ$_{B408}$	This study
BL21(DE3)/pGEX4T2-CspZ$_{B408}$L$_{B379}$	BL21(DE3) producing GST-tagged residues 58 to 720 of CspZ$_{B408}$ except the residues 190 to 213 replaced by residues 190 to 216 from CspZ$_{B379}$	This study
BL21(DE3)/pET15b-DbpA$_{VS461}$	BL21(DE3) producing histidine-tagged residues 22 to 170 of DbpA$_{VS461}$	(64)
BL21(DE3)/pET28a-CspZ-LCAS1	BL21(DE3 producing histidine tagged residue 58 to 711 of CspZ-LCAS1	This study
BL21(DE3)/pET28a-CspZ-LCAS2	BL21(DE3 producing histidine tagged residue 58 to 711 of CspZ-LCAS2	This study

BL21(DE3)/pET28a-CspZ-LCAS3	BL21(DE3 producing histidine tagged residue 58 to 711 of CspZ-LCAS3	This study
BL21(DE3)/pET28a-CspZ-LCAS4	BL21(DE3 producing histidine tagged residue 58 to 711 of CspZ-LCAS4	This study
Rosetta-gami(DE3)	F– ompT hsdSB (rB– mB–) gal dcm lacY1 ahpC (DE3) gor522::Tn10 trxB pRARE (CamR, KanR, TetR)	MilliporeSigma
P. pastoris		
X-33/FH SCR6-7	Wild-type Mut+ Pichia strain for expression of FH SCR6-7 (residues 321 to 444 of human FH)	Invitrogen
Plasmids		
pJET1.2/Blunt	AmpR[a]; PCR cloning vector	ThermoFisher
pGEX4T2	AmpR; GST-tagged protein expression vector	Qiagen
pGEX4T2-CspZ	AmpR; pGEX4T2 encoding GST fusion protein residue 58 to 711 of CspZ	(2)
pGEX4T2-CspZ- $CspZ_{B379}$	AmpR; pGEX4T2 encoding GST fusion protein residue 58 to 723 of $CspZ_{B379}$	This study
pGEX4T2-CspZ- $CspZ_{B408}$	AmpR; pGEX4T2 encoding GST fusion protein residue 58 to 720 of $CspZ_{B408}$	This study
pGEX4T2-CspZ-$CspZ_{B379}L_{B408}$	AmpR; pGEX4T2 encoding GST fusion protein residue 58 to 723 of $CspZ_{B379}$ except the residues 190 to 216 replaced by residues 190 to 213 from $CspZ_{B408}$	This study
pGEX4T2-CspZ-$CspZ_{B408}L_{B379}$	AmpR; pGEX4T2 encoding GST fusion protein residue 58 to 720 of $CspZ_{B408}$ except the residues 190 to 213 replaced by residues 190 to 216 from $CspZ_{B379}$	This study
pET28a	KanR[b]; Histidine-tagged protein expression vector	EMD Millipore

pET28a-CspZ-LCAS1	KanR; pET28a encoding histidine protein residues 58 to 711 of the CspZ-LCAS1	This study
pET28a-CspZ-LCAS2	KanR; pET28a encoding histidine protein residues 58 to 711 of the CspZ-LCAS2	This study
pET28a-CspZ-LCAS3	KanR; pET28a encoding histidine protein residues 58 to 711 of the CspZ-LCAS3	This study
pET28a-CspZ-LCAS4	KanR; pET28a encoding histidine protein residues 58 to 711 of the CspZ-LCAS4	This study
pKFSS-1	$StrR^c$; *Borrelia* shuttle vector	(65)
pKFSS/pCspZ$_{B31}$	StrR; pKFSS-1 encoding intact *cspZ$_{B31}$*, driven by the promoter of *cspZ$_{B31}$*	(2)
pKFSS/pCspZ$_{B379}$	StrR; pKFSS-1 encoding intact *cspZ$_{B379}$*, driven by the promoter of *cspZ$_{B31}$*	This study
pKFSS/pCspZ$_{B408}$	StrR; pKFSS-1 encoding intact *cspZ$_{B408}$*, driven by the promoter of *cspZ$_{B31}$*	This study
pKFSS/pCspZ$_{B379}$L$_{B408}$	StrR; pKFSS-1 encoding intact *cspZ$_{B379}$* except the residues 190 to 216 replaced by residues 190 to 213 from *cspZ$_{B408}$*, driven by the promoter of *cspZ$_{B31}$*	This study
pKFSS/pCspZ$_{B408}$L$_{B379}$	StrR; pKFSS-1 encoding intact *cspZ$_{B408}$* except the residues 190 to 213 replaced by residues 190 to 216 from *cspZ$_{B379}$*, driven by the promoter of *cspZ$_{B31}$*	This study
pETm-11/pCspZ$_{B379}$	KanR; 6xHis tag expression vector encoding CspZ$_{B379}$ residues 23-236	This study
pETm-11/pCspZ$_{B408}$	KanR; 6xHis tag expression vector encoding CspZ$_{B408}$ residues 23-236	This study
pPICZα-FH		This study

		Zeocin resistant; yeast expression vector encoding SCR6-7 of human FH under αMF secretion signal

320 [a]Ampicillin resistant
321 [b]Kanamycin resistant
322 [c]Streptomycin resistant

Table S8. Primers used in this study.

Purpose	Primer	Sequence
qPCR spirochete burden: *recA*	BBRecAfp	GTGGATCTATTGTATTAGATGAGGCTCTCG
	BBRecArp	CAGCAACATGTCTGGCATTAGACAC
qPCR for mouse samples: *mouse nidogen*	mNidfp	CCAGCCACAGAATCCCATCC
	mNidrp	GGACATACTCTGCTGCCATC
qPCR for quail samples: *quail β-actin*	qß-actinfp	CTGGCACCTAGCACAATGAA
	qß-actinfp	CTGCTTGCTGATCCACATCT
qPCR dosage effects: *colE1*	BBColE1fp	CTACATACCTCGCTCTGCTAATC
	BBColE1rp	CGAAACCCGACAGGACTATAAA
qPCR dosage effects: *bbh17*	BBBbh17fp	AACACTATCTTAAATGTCCCCCACAA
	BBBbh17rp	GTGGAAGAGTGGTTATGGTCAATTTT
Generate $_{B379}L_{B408}$: SLIM step 1	$_{B379}L_{B408}$_A-1_mtsengtd	CAGAAGATGTGTTACCTTCCGAAGTCATATAAGTCATAATATC ATTATATGCTCCTGTA
	$_{B379}L_{B408}$_B-1_mtsengtd	TATGACTTATATGACTTCGGAAGGTAACACATCTTCTGATAAA AGTAAGGTTAATCAAG
	$_{B379}L_{B408}$_C-1_mtsengtd	ATATCATTATATGCTCCTGTA
	$_{B379}L_{B408}$_D-1_mtsengtd	ATAAAAGTAAGGTTAATCAAG
Generate $_{B379}L_{B408}$: SLIM step 2	$_{B379}L_{B408}$_A-2_tsenngtd	TTTTATCAGAATCTGTGTTATTACCTTCCGAAGTATAAGTCATA ATATCATTATATGCTCCTGTA
	$_{B379}L_{B408}$_B-2_tsenngtd	TATGACTTATACTTCGGAAGGTAATAACACAGATTCTGATAAA AGTAAGGTTAATCAAGCTATAT
	$_{B379}L_{B408}$_C-2_tsenngtd	ATATCATTATATGCTCCTGTA
	$_{B379}L_{B408}$_D-2_tsenngtd	GTAAGGTTAATCAAGCTATAT
Generate $_{B379}L_{B408}$: SLIM step 3	$_{B379}L_{B408}$_A-3_sevnnvtd	CAGAATCTGTAACGTTATTAACTTCCGAATAAGTCATAATATCA TTATATGCTCCTGTA

	$_{B379}L_{B408}$_B-3_sevnnvtd	TATGACTTATTCGGAAGTTAATAACGTTACAGATTCTGATAAA AGTAAGGTTAATCAAG
	$_{B379}L_{B408}$_C-3_sevnnvtd	ATATCATTATATGCTCCTGTA
	$_{B379}L_{B408}$_D-3_sevnnvtd	ATAAAAGTAAGGTTAATCAAG
Generate $_{B408}L_{B379}$: SLIM step 1	$_{B408}L_{B379}$_A-1_tsenngtd	CAGAATCTGTACCGTTATTTTCCGAAGTATAAGTCATAATATCA TTATATGCTTCTGTA
	$_{B408}L_{B379}$_B-1_tsenngtd	TATGACTTATACTTCGGAAAATAACGGTACAGATTCTGATAAA AGTAAGGTTAATCAAG
	$_{B408}L_{B379}$_C-1_tsenngtd	ATATCATTATATGCTTCTGTA
	$_{B408}L_{B379}$_D-1_tsenngtd	TAAAAGTAAGGTTAATCAAG
Generate $_{B408}L_{B379}$: SLIM step 2	$_{B408}L_{B379}$_A-2_mtsengts	TTTTATCAGAAGATGTACCGTTTTCCGAAGTCATATAAGTCATA ATATCATTATATGCTTCTGTA
	$_{B408}L_{B379}$_B-2_mtsengts	TATGACTTATATGACTTCGGAAAACGGTACATCTTCTGATAAA AGTAAGGTTAATCAAGCTATAT
	$_{B408}L_{B379}$_C-2_mtsengts	ATATCATTATATGCTTCTGTA
	$_{B408}L_{B379}$_D-2_mtsengts	GTAAGGTTAATCAAGCTATAT
Generate $_{B408}L_{B379}$: SLIM step 3	$_{B408}L_{B379}$_A-3_imtysegts	AAGATGTACCTTCCGAATAAGTCATAATATAAGTCATAATATC ATTATATGCTTCTGTA
	$_{B408}L_{B379}$_B-3_imtysegts	TATGACTTATATTATGACTTATTCGGAAGGTACATCTTCTGATA AAAGTAAGGTTAATC
	$_{B408}L_{B379}$_C-3_imtysegts	ATATCATTATATGCTTCTGTA
	$_{B408}L_{B379}$_D-3_imtysegts	CTGATAAAAGTAAGGTTAATC
Generate $CspZ_{B379}$ residues 23-236 or $CspZ_{B408}$ residues 23-236	*cspZ* Forw.	CATGCCATGGGCAGATTAAATCAGAGAAAT
	cspZ Rev.	GCTTGCGGCCGCTTATAATAAAGTTTGCTTAAT

324

Table S9. Data processing, refinement, and validation statistics of crystal structures.

Dataset	**CspZ$_{B408}$**	**CspZ$_{B379}$**	**CspZ$_{B408}$-SCR6-7**
X-ray diffraction data			
PDB entry	7ZJK	7ZJJ	7ZJM
Beamline	BESSY II beamline 14.1	BESSY II beamline 14.1	BESSY II beamline 14.1
Space group	$P2_1$	$P22_12_1$	$P2_12_12_1$
a, b, c (Å)	47.63, 87.49, 48.86	53.60, 59.95, 61.05	42.10, 71.07, 147.75
α, β, γ (°)	90.0, 97.1, 90.0	90.0, 90.0, 90.0	90.0, 90.0, 90.0
Wavelength (Å)	0.9798	0.9762	0.9798
Resolution (Å)	48.49-2.45	61.05-2.10	73.87-2.59
Highest resolution bin (Å)	2.55-2.45	2.16-2.10	2.65-2.59
No. of reflections	97062	127094	101717
No. of unique reflections	14406	11805	14404
Completeness (%)	98.2 (88.4)[a]	98.9 (99.5)	99.8 (99.8)
R_{merge}	0.09 (0.38)	0.10 (0.35)	0.11 (0.38)
$CC_{1/2}$	0.997 (0.940)	0.998 (0.985)	0.988 (0.926)
I/σ (I)	12.1 (4.2)	14.8 (6.3)	12.8 (4.9)
Multiplicity	6.7 (6.2)	10.8 (11.1)	7.1 (7.5)
Refinement			
R_{work}	0.193 (0.248)	0.208 (0.371)	0.217 (0.270)
R_{free}	0.262 (0.399)	0.262 (0.431)	0.275 (0.354)
Average B-factor (Å^2)			
Overall	45.1	33.0	31.9
From Wilson plot	36.9	15.9	24.1
No. of atoms			
Protein	3592	1769	1914
RMS deviations from ideal			
Bond lengths (Å)	0.007	0.008	0.010
Bond angles (°)	1.435	1.541	1.548
Ramachandran outliers (%)			
Residues in most favored regions (%)	93.74	95.31	94.93
Residues in allowed regions (%)	5.10	4.69	4.17
Outliers (%)	1.16	0.00	0.90

[a]Values in parentheses are for the highest resolution bin.

Table S10. pKFSS-1:lp28-3 ratio during *in vitro* culture and in the heart of BALB/c mice and quail at 21dpf[a].

Strain	Copies/500pg DNA[b]			Copies/100ng DNA[c]					
	In vitro			BALB/c Heart			Quail Heart		
B31-A3Δ*cspZ* /	pKFSS	lp28-3	pKFSS/ lp28-3[d]	pKFSS	lp28-3	pKFSS/ lp28-3[f]	pKFSS	lp28-3	pKFSS/ lp28-3
pCspZ$_{B31}$	37173± 6331	43268± 3656	**0.85**	1294± 404	1349± 210	**0.95**	1748± 549	1809± 331	**0.96**
pCspZ$_{B379}$	39782± 7119	41163± 7168	**0.96**	139± 54	133± 15	**1.04**	430± 84	431± 54	**0.99**
pCspZ$_{B408}$	41823± 1686	42614± 12255	**0.98**	927± 126	955± 79	**0.97**	38.5± 7.6	38.1± 7.8	**1.00**
pCspZ$_{B379}$L$_{B408}$	50823± 5142	57618± 15430	**0.88**	1362± 419	1321± 606	**1.03**	15.2± 3.8	14.8± 5.0	**1.02**
pCspZ$_{B408}$L$_{B379}$	37433± 2773	42151± 4658	**0.88**	23.1± 5.1	20.8± 3.6	**1.11**	2658± 416	3145± 1220	**0.84**

[a] Experiment displayed in Figure 3

[b] The copy number of pKFSS or lp28-3 was determined by qPCR; shown are the mean ± SEM from three *in vitro* cultures per spirochete strain

[c] The copy number of pKFSS or lp28-3 was determined by qPCR; shown are the mean ± SEM from the hearts from five BALB/c mice or quail

[d] Ratio of the copy number determined using *colE1* primers to the copy number determined using *bbh17* primers

SUPPLEMENTAL FIGURES

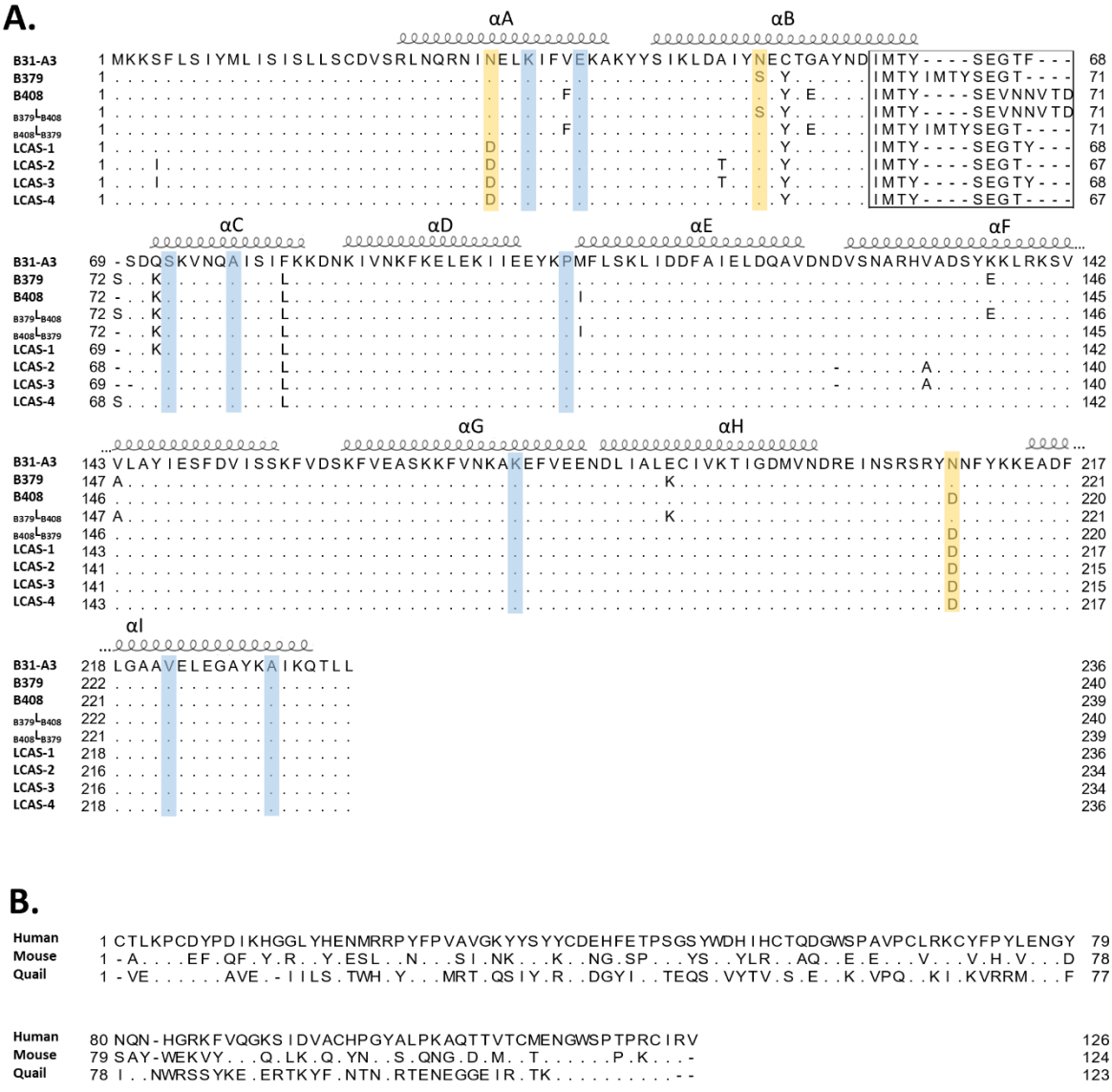

Figure S1. Amino acid alignments of the CspZ and FH variants. Amino acid alignments of **(A)** the indicated CspZ variants, mutants, and reconstructed ancestral states of variants or **(B)** human, mammalian, and avian FH SCR 6-7. The CspZ amino acids accounting for the loop structures are indicated with the box, and the alpha-helices labeled above the sequences are extrapolated from

the high-resolution structure of $CspZ_{B408}$. The yellow and blue shading are indicative of loci showing evidence of positive and negative selection, respectively.

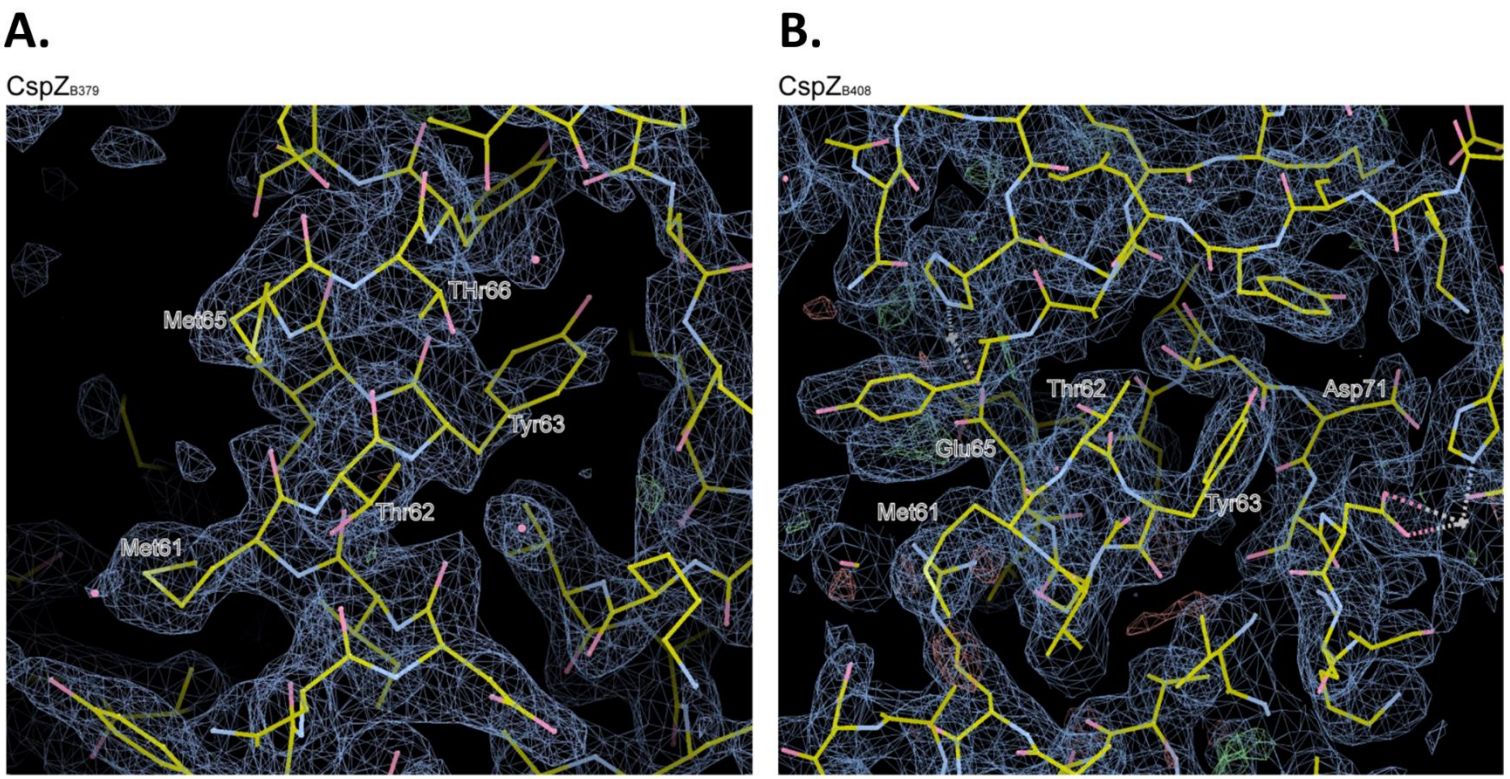

365

366 **Figure S2. Electron density map of crystallization structures.** $2mF_o$-DF_c electron density map contoured at 1.0σ located on

367 α-helix B and the loop region of (**A**) $CspZ_{B379}$ and (**B**) $CspZ_{B408}$, representing protein residues as a stick model.

368

369

370

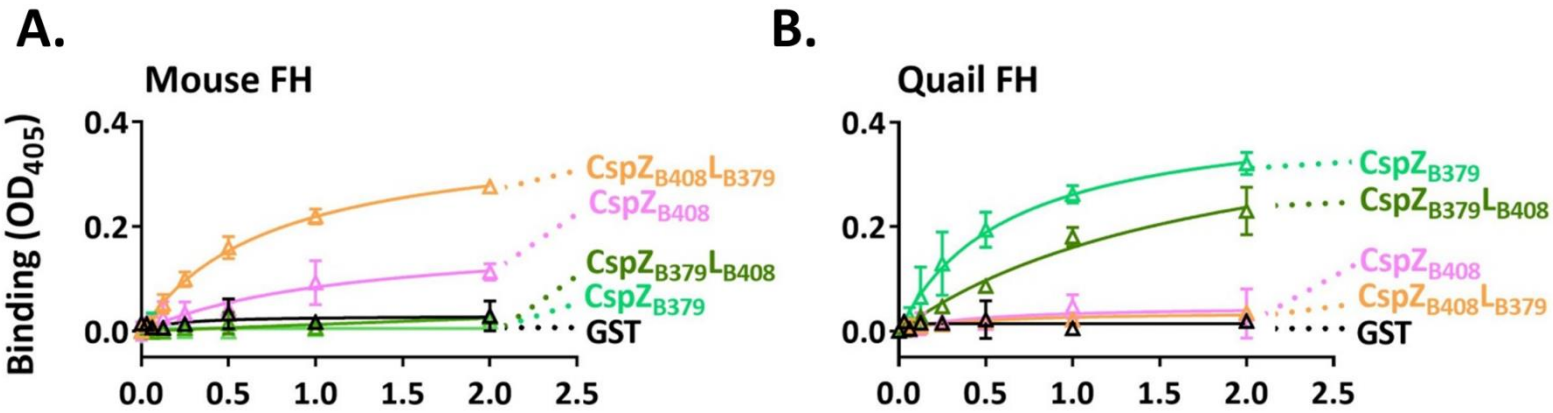

Figure S3. The polymorphic loop structures in recombinant CspZ proteins promote host-specific FH-binding ability determined by ELISA. The indicated concentrations of recombinant GST-tagged $CspZ_{B379}$, $CspZ_{B408}$, $CspZ_{B379}L_{B408}$, or $CspZ_{B408}L_{B379}$, or GST (negative control) were added to triplicate wells coated with FH from mouse or quail, and protein binding was quantitated by ELISA. The experiments were performed with a single preparation of recombinant proteins tested in three independent iterations, in which samples were ran in duplicate. The K_D values **(Table S2)** representing the FH-binding affinity of each protein were determined from the average of three experiments. Shown is a representative iteration averaging the duplicates.

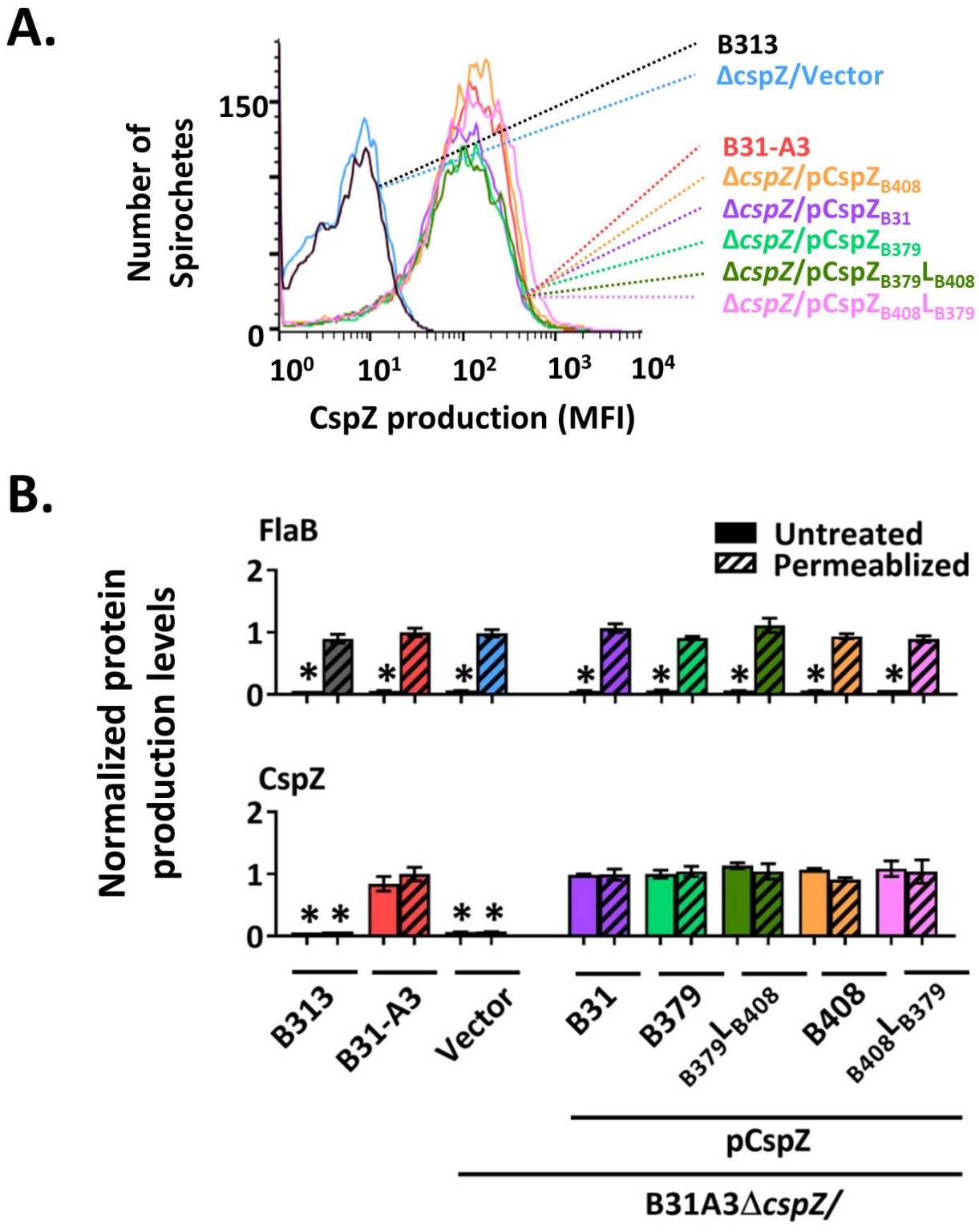
A.
Number of Spirochetes
150
0
10^0 10^1 10^2 10^3 10^4
CspZ production (MFI)
B313
ΔcspZ/Vector
B31-A3
ΔcspZ/pCspZB408
ΔcspZ/pCspZB31
ΔcspZ/pCspZB379
ΔcspZ/pCspZB379LB408
ΔcspZ/pCspZB408LB379
B.
Normalized protein production levels
FlaB
Untreated
Permeablized
2
1
0
CspZ
B313
B31-A3
Vector
B31
B379
B379LB408
B408
B408LB379
pCspZ
B31A3ΔcspZ/

382

Figure S4. Indistinguishable surface production of CspZ among *B. burgdorferi* strains was observed using flow cytometry. Flow cytometry analysis of CspZ localized on the surface of *B. burgdorferi* strains B31-A3, B31-A3Δ*cspZ* harboring the vector pKFSS ("Δ*cspZ*/Vector"), or this *cspZ* mutant strain producing $CspZ_{B31}$, $CspZ_{B379}$, $CspZ_{B379}L_{B408}$, $CspA_{B408}$, or $CspZ_{B408}L_{B379}$. **(A)** Representative histograms of flow cytometry analysis showing the levels of CspZ surface production on the indicated strains. **(B)** The production of FlaB (negative control) and CspZ on the surface of indicated *B. burgdorferi* strains was detected by flow cytometry. Values are shown normalized to the production levels of FlaB or CspZ on the surface of permeabilized B31-A3. Each bar represents the mean of four independent experiments ± the standard deviation. An asterisk (*) indicates that relative surface production of the indicated proteins was significantly lower ($p < 0.05$, Kruskal-Wallis test with the two-stage step-up method of Benjamini, Krieger, and Yekutieli) than that of permeabilized FlaB or CspZ by B31-A3.

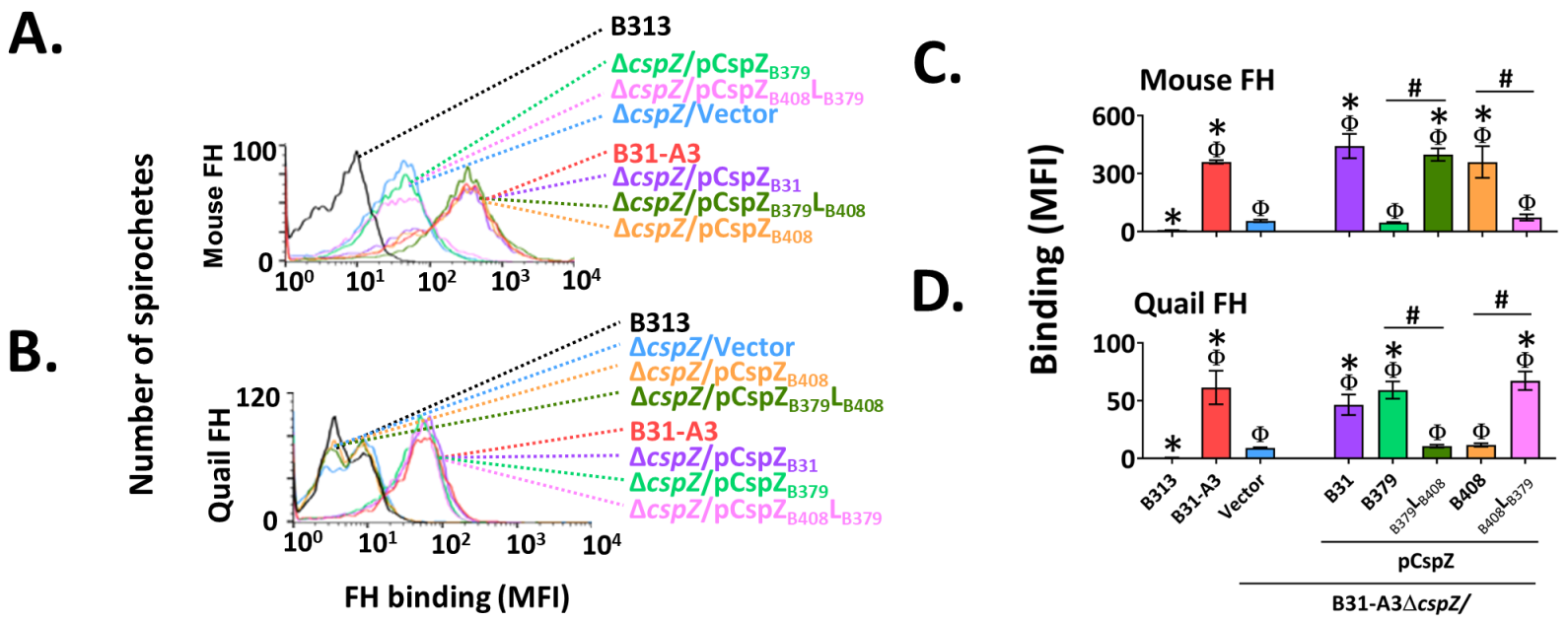

405

406 **Figure S5. The polymorphic CspZ loop determines the host-specific, allelically variable FH-binding activity on spirochete**

407 **surface.** *B. burgdorferi* strains B313 (negative control), B31-A3, B31-A3Δ*cspZ* harboring the empty vector pKFSS

408 ("Δ*cspZ*/Vector"), or this mutant strain producing $CspZ_{B31}$, $CspZ_{B379}$, $CspZ_{B379}L_{B408}$, $CspZ_{B408}$, or $CspZ_{B408}L_{B379}$, was incubated

409 with mouse or quail FH. The bacteria were stained with antibodies that recognize these FH variants prior to flow cytometry.

410 Shown are the representative histograms of flow cytometry analysis presenting the levels of FH from **(A)** mouse or **(B)** quail

411 binding to each *B. burgdorferi* strain. The levels of **(C)** mouse or **(D)** quail FH-binding were measured by flow cytometry and

412 presented as mean fluorescence index (MFI). Each bar represents the mean of three independent experiments ± SEM. Significant

differences ($p < 0.05$, Kruskal-Wallis test with the two-stage step-up method of Benjamini, Krieger, and Yekutieli) in the levels of FH-binding relative to the B313/Vector ("Φ"), Δ*cspZ*/Vector ("*"), or between two strains relative to each other ("#") are indicated.

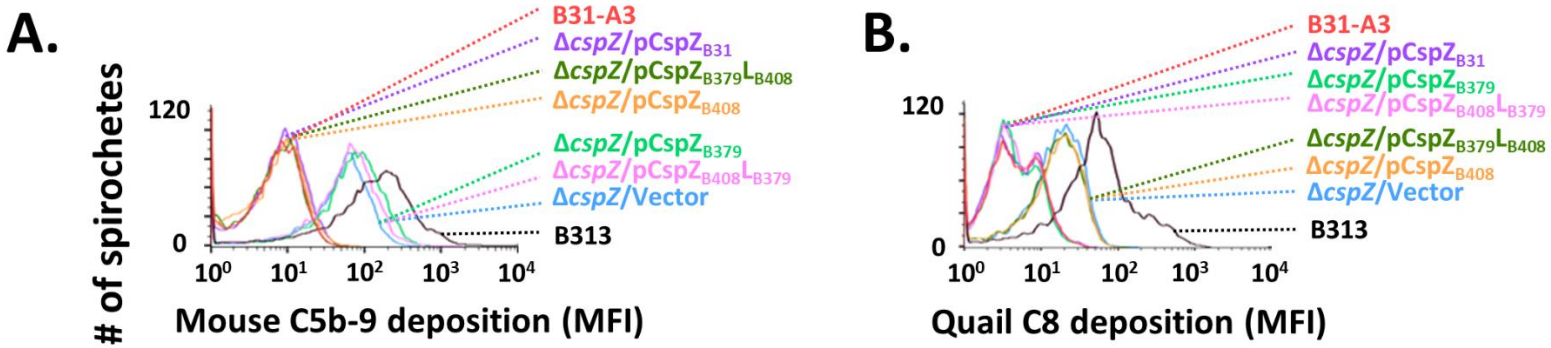

Figure S6. The CspZ loop-driven, variable FH-binding activity reduces host-specific complement deposition. *B. burgdorferi* strains B313 (negative control), B31-A3, B31-A3Δ*cspZ* harboring the empty vector pKFSS-1 ("Δ*cspZ*/Vector"), or this mutant strain producing $CspZ_{B31}$, $CspZ_{B379}$, $CspZ_{B379}L_{B408}$, $CspZ_{B408}$, or $CspZ_{B408}L_{B379}$, was incubated with 20% (**A**) mouse or (**B**) quail sera, followed by straining with antibodies against mouse C5b-9 or quail C8. Shown are the representative histograms of flow cytometry analysis presenting the deposition levels of **(A)** mouse C5b-9 or **(B)** quail C8 on the surface of the indicated strains.

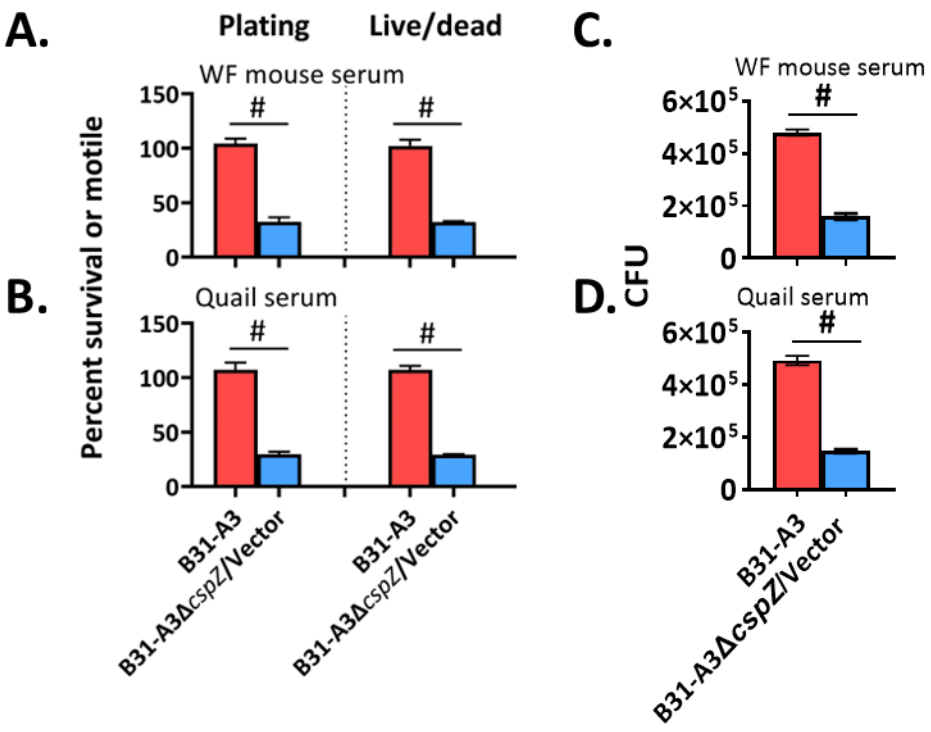

442

443 **Figure S7. No difference of *B. burgdorferi* strains survival in white-footed mouse and quail**
444 **sera determined by colony forming units on agar plates vs. Live/Dead staining.** The indicated
445 *B. burgdorferi* strains were incubated for 4-h with **(A and C)** white-footed mouse, **(B and D)** quail,
446 to a final concentration of 40%. The spirochete survival was obtained by counting the CFU on the
447 agar plates ("Plating") or applying live/dead staining and microscopically counting the number of
448 live spirochetes ("Live/dead"). **(A and B)** The percentage of survival was calculated using the
449 number of colony forming units or the number of live spirochetes at 4-h post incubation normalized
450 to that prior to the incubation with serum (0-h). **(C and D)** The number of CFU of the spirochetes
451 determined by plating the spirochete-sera mixtures at 4-h post incubation were shown. Each bar
452 represents the mean of three independent experiments (n = 3) ± SEM. Significant differences ($p < 0.05$, Mann-Whitney test) in the percent survival between spirochetes strains are indicated ("#").

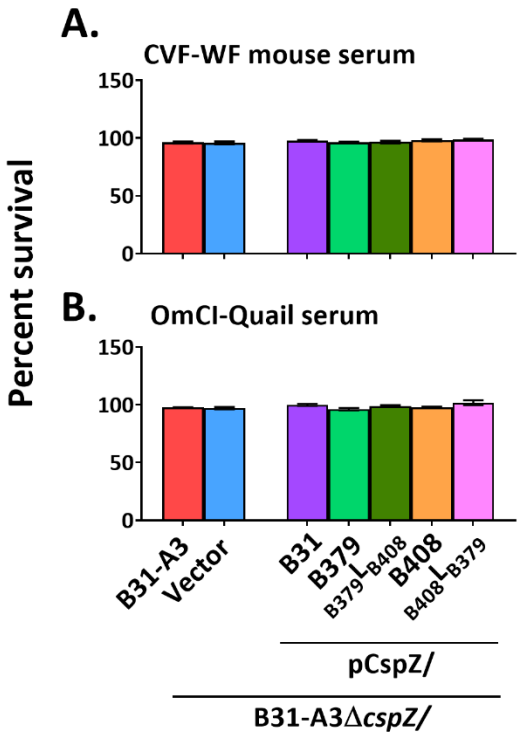

Figure S8. The CspZ loop-driven, host-specific serum resistance is recovered in complement-depleted sera. The indicated *B. burgdorferi* strains were incubated for 4-h with complement-depleted (**A**) mouse ("CVF-WF mouse serum") or (**B**) quail ("OMCI-quail serum") sera, to a final concentration of 40%. The levels of spirochete survival were determined by applying live/dead staining and microscopically counting the number of live spirochetes. The percentage of survival was calculated using the number of live spirochetes at 4-h post incubation normalized to that prior to the incubation with serum (0-h). Each bar represents the mean of three independent experiments (n = 3) ± SEM. Significant differences ($p < 0.05$, Mann-Whitney test) in the percent survival between spirochetes strains are indicated ("#").

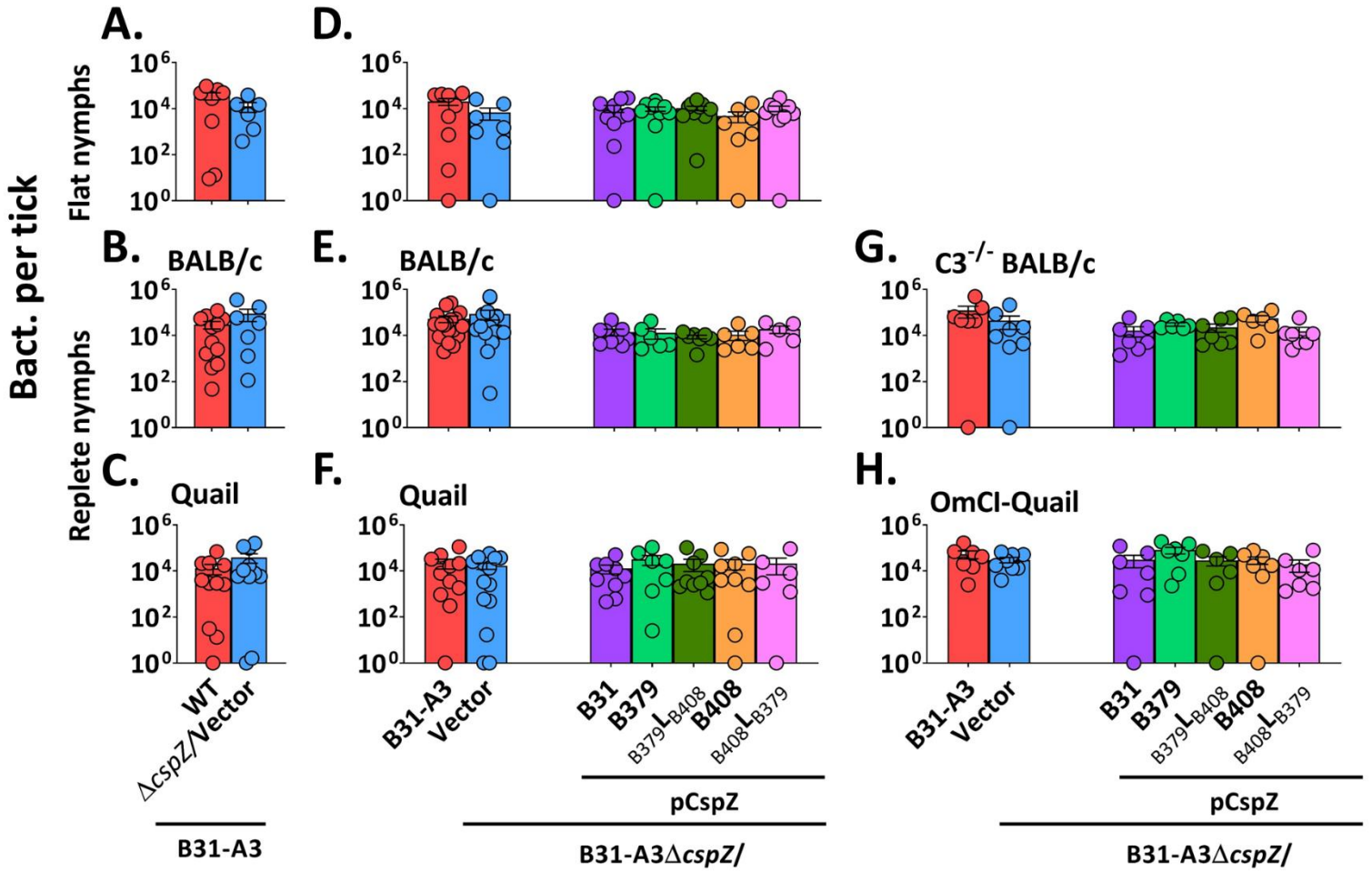

Figure S9. *B. burgdorferi* strains exhibit similar burdens in flat and fed nymphs. *B. burgdorferi*-infected **(A)** flat nymphs were allowed to feed to repletion on **(B, E)** BALB/c or **(G)** C3-/- BALB/c mice, or **(C, F)** quail or **(H)** OmCI-treated quail. The

spirochete loads in **(A, D)** flat or **(B, C, E, F, G, H)** replate nymphs were determined by qPCR. Shown are the geometric mean ± geometric standard deviation of at least five nymphs per group. There was no statistical difference ($p > 0.05$) of the spirochete burdens between different groups of the replete ticks using a **(A to C)** Mann-Whitney test or **(D to H)** Kruskal-Wallis test with the two-stage step-up method of Benjamini, Krieger, and Yekutieli.

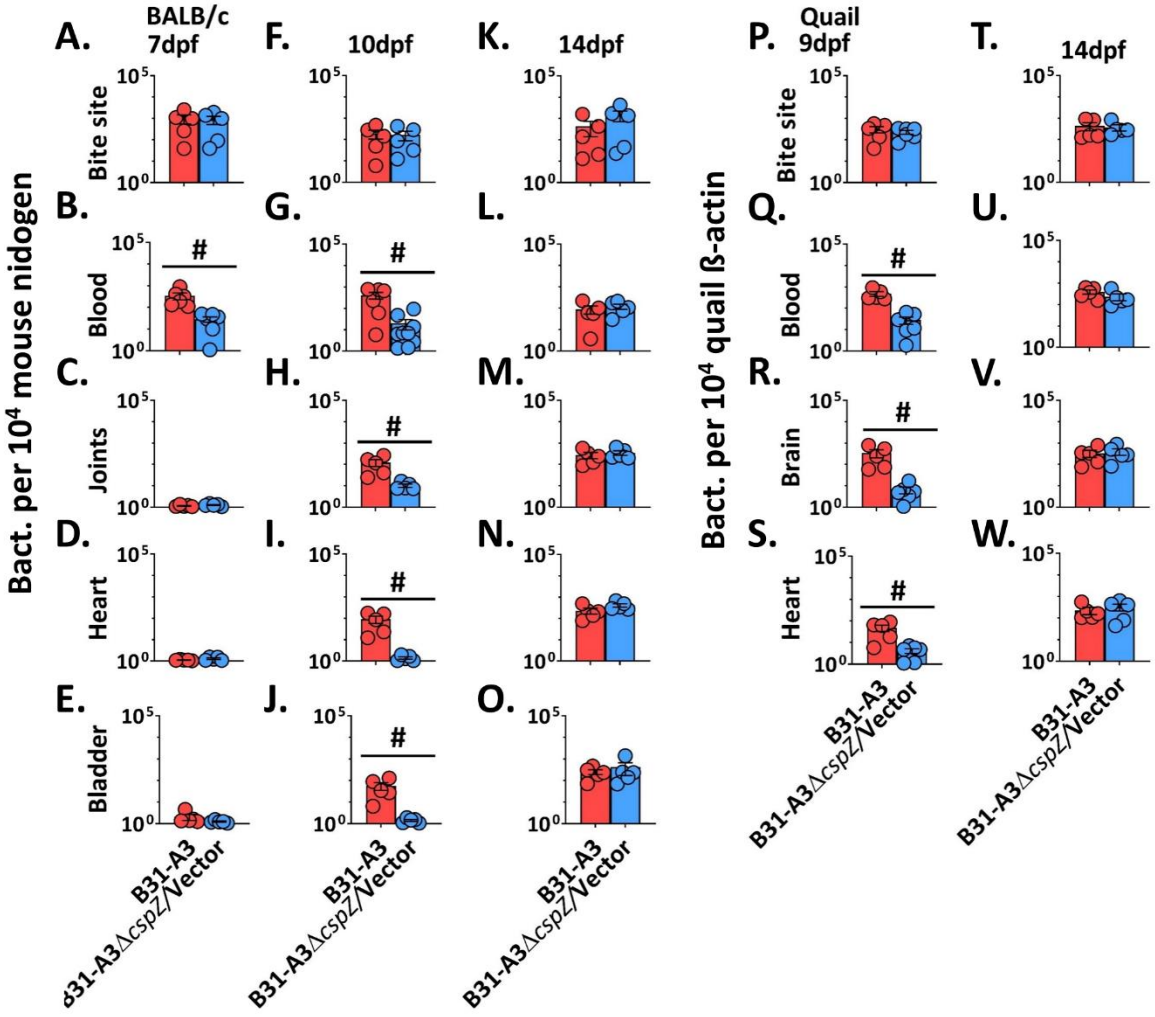

Figure S10. CspZ facilitates early bacteremia and distal tissue colonization during tick infection. The *I. scapularis* nymphs carrying *B. burgdorferi* strain B31-A3 or B31-A3Δ*cspZ* harboring the vector pKFSS ("Δ*cspZ*/Vector") were allowed to feed until repletion on **(A to O)** BALB/c mice or **(P to W)** quail. The mice were euthanized at **(A to E)** 7, **(F to J)** 10, or **(K to O)** 14 days post nymphs feeding (dpf), whereas the quail were euthanized at **(P to S)** 9 or **(T to W)** 14dpf. **(A, F, K)** The site of the skin where nymphs fed ("Bite site"), **(B, G, L)** blood, **(C, H, M)** tibiotarsus joints, **(D, I, N)** heart, and **(E, J, O)** bladder of mice; and **(P, T)** the bite site, **(Q, U)** blood, **(R, V)** brain, and **(S, W)** heart of quail, were collected immediately after euthanasia and

spirochete loads were determined by qPCR. The *recA* copies were normalized to 10^4 copies of **(A to O)** mouse nidogen or **(P to W)** quail β-actin. Shown are the geometric mean of bacterial loads ± SEM of five animals per group, except for all tissues from quail infected with Δ*cspZ*/Vector at 9dpf, which has six. Significant differences ($p < 0.05$, Mann-Whitney test) in the spirochete burdens between two strains relative to each other are indicated ("#").

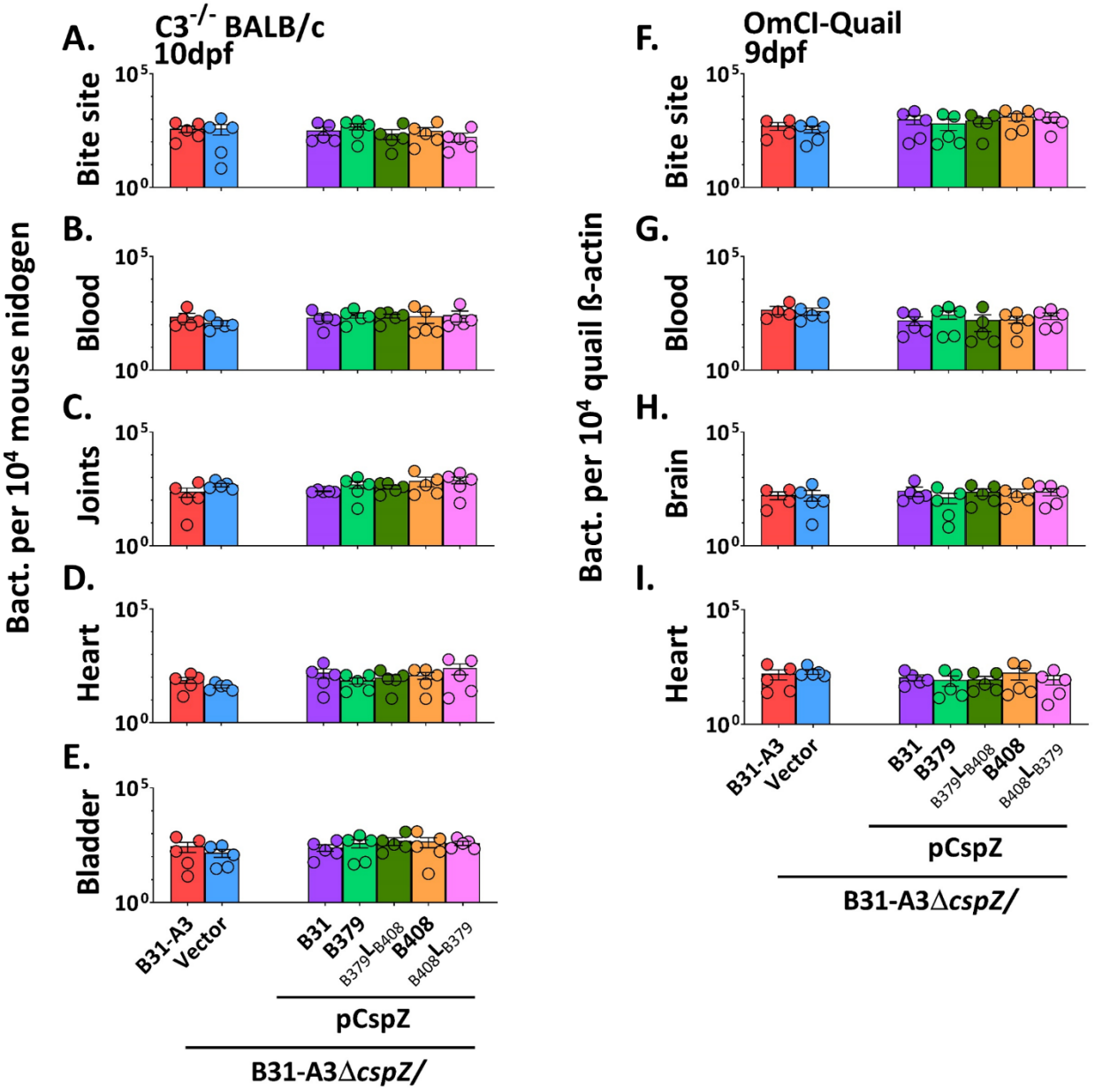

Figure S11. The CspZ loop-mediated early hematogenous dissemination is recovered when complement is depleted from hosts. *I. scapularis* nymphs carrying B31-A3, B31-A3Δ*cspZ* harboring the empty vector pKFSS ("Δ*cspZ*/Vector"), or this *cspZ* mutant strain producing $CspZ_{B31}$, $CspZ_{B379}$, $CspZ_{B379}L_{B408}$, $CspZ_{B408}$, or $CspZ_{B408}L_{B379}$ were allowed to feed until repletion on **(A to E)** $C3^{-/-}$ mice in a BALB/c background or **(F to I)** OmCI-treated quail, both of which

deplete complement in the respective hosts. The *recA* copies in the indicated distal tissues were normalized to 10^4 copies of **(A to E)** mouse nidogen at 10 days post nymphs feeding (dpf), or **(F to I)** quail β-actin, at 9dpf. Shown are the geometric mean of bacterial loads ± SEM of five animals per group. There were no significant differences ($p < 0.05$, Kruskal-Wallis test with the two-stage step-up method of Benjamini, Krieger, and Yekutieli) in the spirochete burdens for any strain.

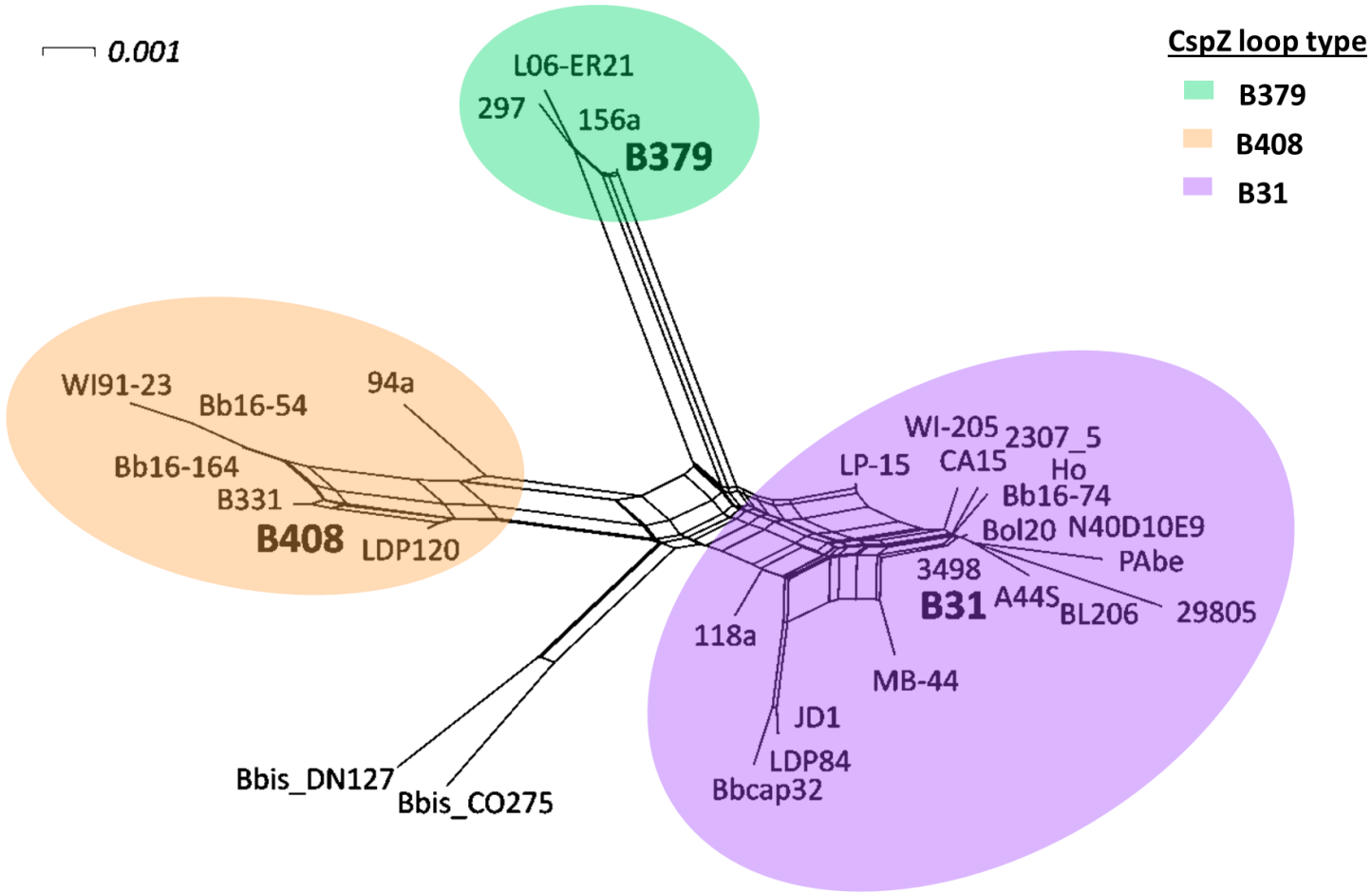

Figure S12. Phylogenetic network of *cspZ* haplotypes. Edges are colored based on their loop structure ($CspZ_{B379}$, $CspZ_{B408}$, and $CspZ_{B31}$ in green, orange, and purple, respectively).

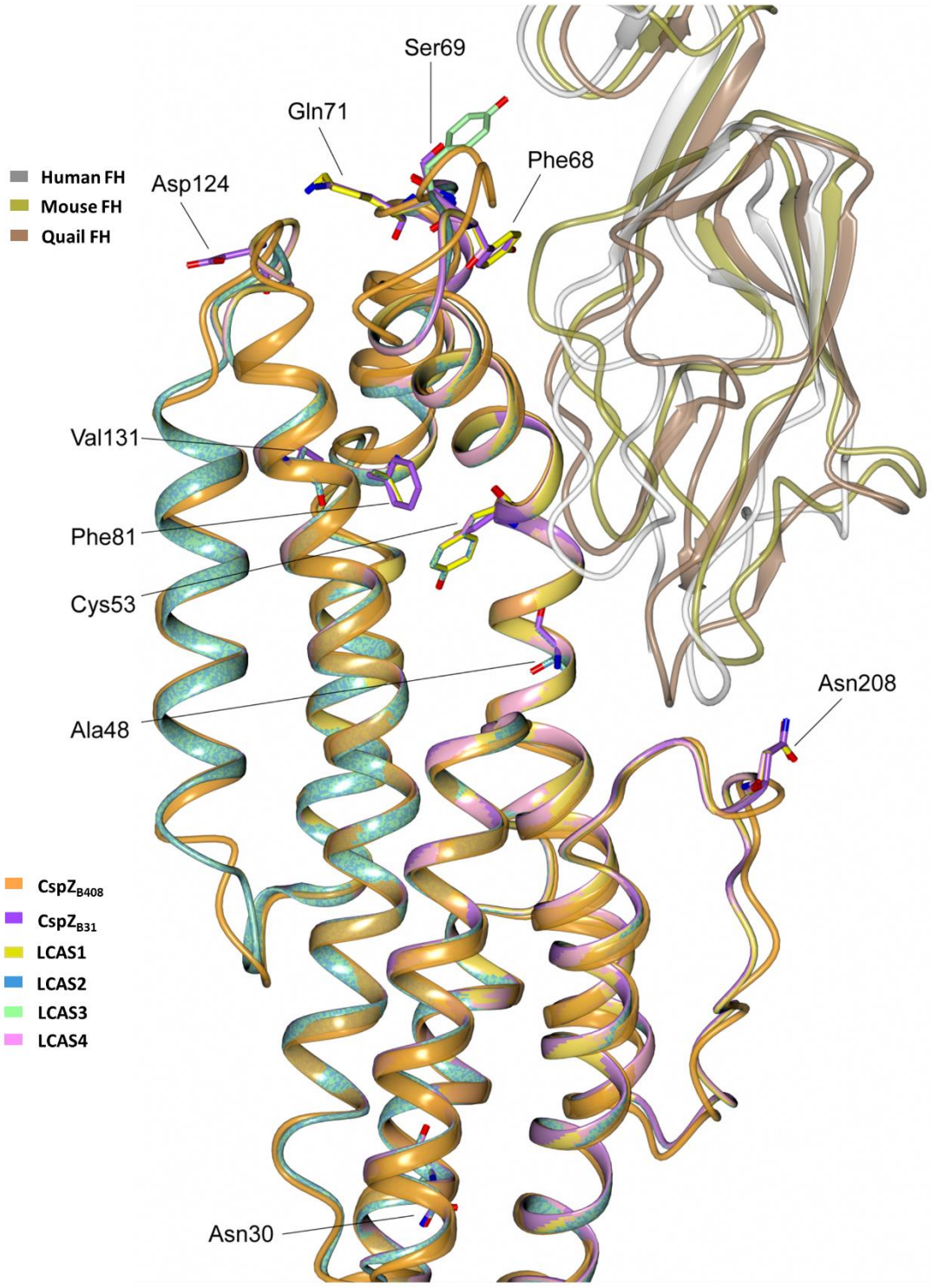
Ser69
Gln71
Phe68
Asp124
Human FH
Mouse FH
Quail FH
Val131
Phe81
Cys53
Asn208
Ala48
CspZB408
CspZB31
LCAS1
LCAS2
LCAS3
LCAS4
Asn30

549

550

Figure S13. The CspZ last common ancestor states are predicted to bind multiple types of FH. The crystal structure of $CspZ_{B408}$-SCR6-7 where human SCR6-7 (grey) is superimposed with mouse FH SCR6-7 (gold, PDB: 2YBY) and the predicted structure of quail SCR6-7 (brown). $CspZ_{B408}$ (orange) is superimposed with $CspZ_{B31}$ (purple) and the last common ancestor states: LCAS1 (yellow), LCAS2 (blue), LCAS3 (green), and LCAS4 (pink). Residues that differ between $CspZ_{B31}$ and the LCAS variants are labelled.

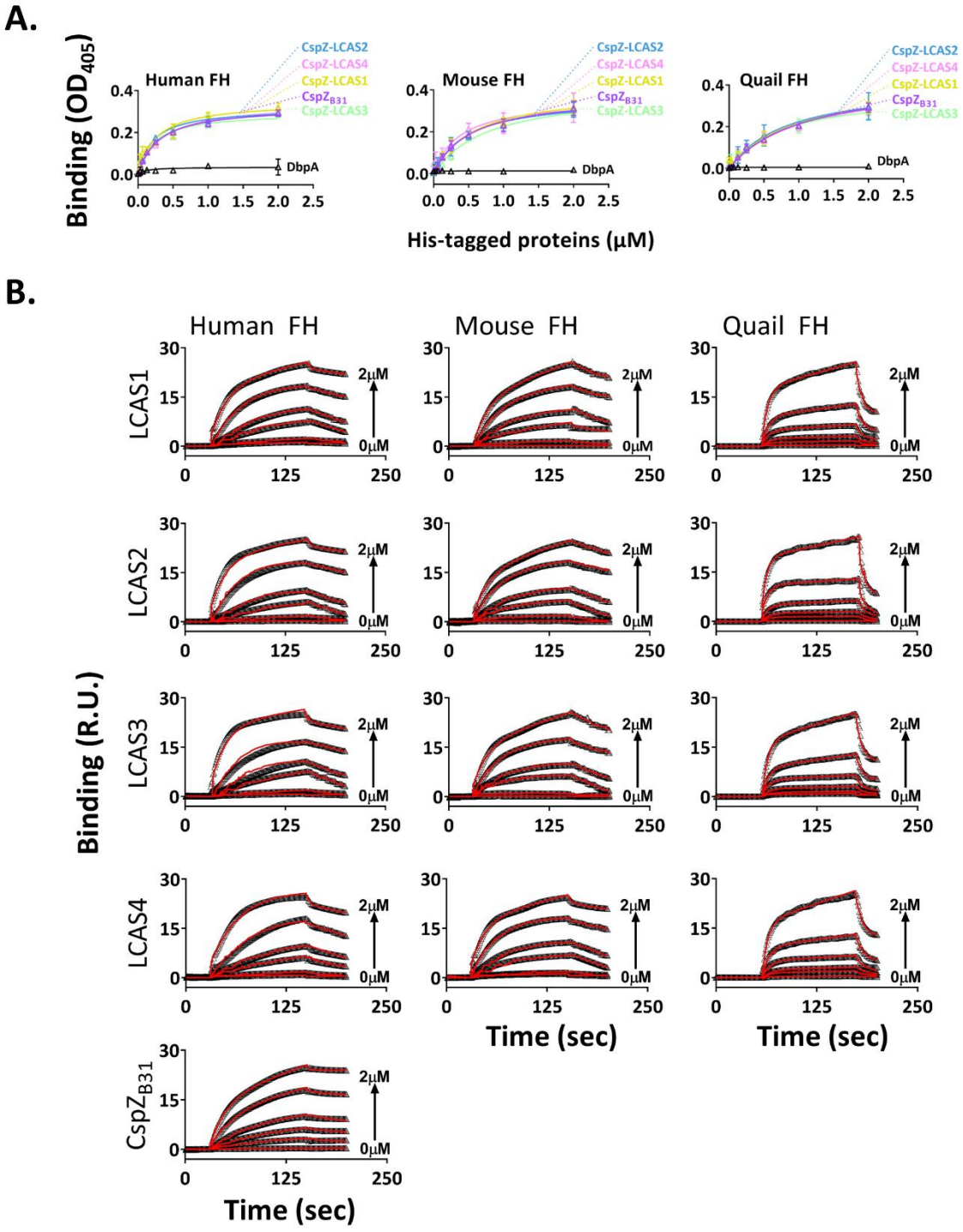

573

574 **Figure S14. The predicted last common ancestor states of CspZ bind to human, mouse, and**

575 **quail FH. (A)** The indicated concentrations of recombinant histidine-tagged last common ancestor

states of CspZ or DbpA (negative control) were added to triplicate wells coated with FH, and protein binding was quantitated by ELISA. The experiments were performed with a single preparation of recombinant proteins tested in three independent iterations, in which samples were ran in duplicate. The K_D values **(Table S6)** representing the FH-binding affinity of each protein were determined from the average of three experiments. Shown is a representative iteration averaging the duplicates. **(B)** Ten micrograms FH were conjugated on a SPR chip. 0.008 to 2μM of the CspZ ancestor states or $CspZ_{B31}$ (control) was flowed over the chip surface. Binding was measured in response units (RU) by SPR. The experiments were performed with a single preparation of recombinant proteins tested in three independent replicates with samples ran in duplicate. Shown is one representative experiment. The k_{on}, k_{off}, and K_D values were determined from the average of these three experiments (**Table S6**).

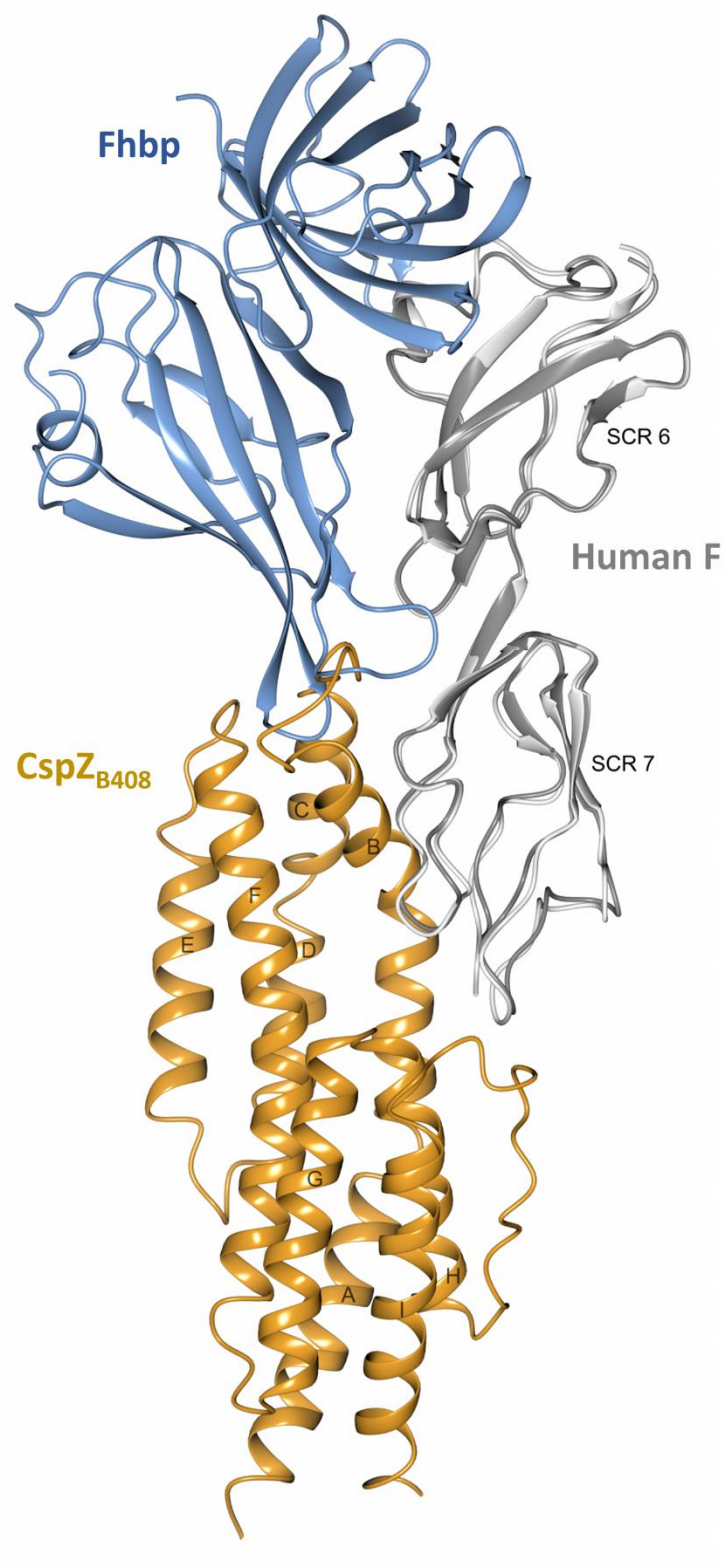

596

Figure S15. Structural comparison between $CspZ_{B408}$-human SCR6-7 and the *N. meningitidis* Fhbp-human SCR6-7 complexes. Human FH SCR6-7 (light grey) from the complex structure with $CspZ_{B408}$ (orange) was superimposed with human FH SCR6-7 (dark grey) from the complex structure with Fhbp (dark blue, PDB: 2W81), the FH-binding protein from *N. meningitidis*. α-helices in $CspZ_{B408}$ are labelled from A to I starting from the N-terminus.

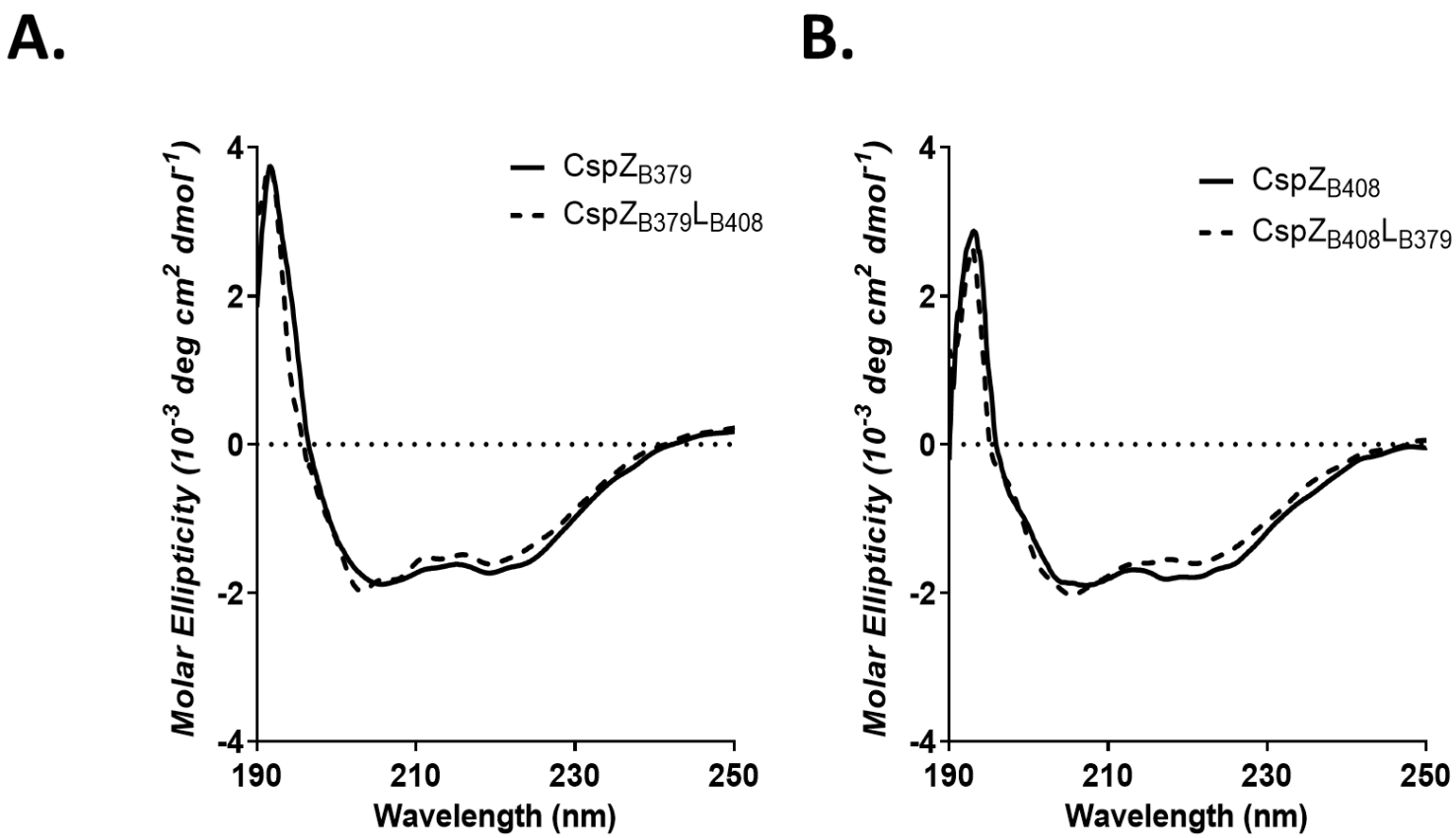

Figure S16. CD spectra demonstrate no impacts of secondary structures by swapping the loops. Far-UV CD analysis of $CspZ_{B379}$, $CspZ_{B408}$, $CspZ_{B379}L_{B408}$, and $CspZ_{B408}L_{B379}$. The molar ellipticity, Φ, was measured from 190-250nm for 10μM of each protein in PBS.

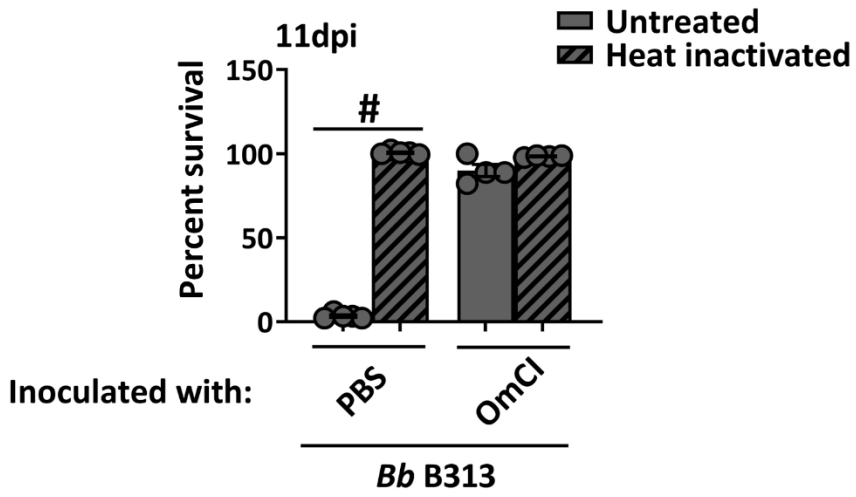

Figure S17. OmCI prevents quail serum-mediated killing of a complement-sensitive spirochete strain at 11 days post injection. *Coturnix* quail were subcutaneously inoculated with OmCI (1mg/kg of quail) or PBS buffer. Untreated (filled bars) or heat-treated (hatched bars) sera collected from these quail at 11 days post inoculation (dpi) were incubated with a serum-sensitive, highly passaged *B. burgdorferi* strain B313. The number of live spirochetes were quantified microscopically using live/dead staining, and the survival percentage of the spirochetes was calculated using the number of live spirochetes at 4-h post incubation normalized to that at 0-h. Each bar represents the mean ± SEM of three independent experiments from sera from four quail per group. Significant differences ($p < 0.05$, Mann-Whitney test) in the percentage survival of spirochetes are indicated ("#").

SUPPLEMENTAL REFERENCES

1. T. Hart *et al.*, Polymorphic factor H-binding activity of CspA protects Lyme borreliae from the host complement in feeding ticks to facilitate tick-to-host transmission. *PLoS pathogens* **14**, e1007106 (2018).
2. A. L. Marcinkiewicz *et al.*, Blood treatment of Lyme borreliae demonstrates the mechanism of CspZ-mediated complement evasion to promote systemic infection in vertebrate hosts. *Cellular microbiology* **21**, e12998 (2019).
3. A. M. Frye *et al.*, A soft tick *Ornithodoros moubata* salivary protein OmCI is a potent inhibitor to prevent avian complement activation. *Ticks and tick-borne diseases* **11**, 101354 (2020).
4. M. Combs *et al.*, Phylogenomic Diversity Elucidates Mechanistic Insights into Lyme Borreliae-Host Association. *mSystems* **7,** e0048822 (2022).
5. Y. P. Lin, Tufts, D.M., Combs, M., Dupuis II, A.P., Marcinkiewicz, A.L., Hirsbrunner, A.D., Diaz, A.J., Stout, J.L., Blom, A.M., Strle, K., Davis, A.D., Kramer, L.D., Kolokotronis, S.O., Diuk-Wasser, M.A., Cellular and immunological mechanisms influence host-adapted phenotypes in a vector-borne microparasite. *Proc. Biol. Sci.* **289,** 20212087 (2022).
6. M. B. Lawrenz *et al.*, Human antibody responses to VlsE antigenic variation protein of *Borrelia burgdorferi*. *Journal of clinical microbiology* **37**, 3997-4004 (1999).
7. S. R. Casjens *et al.*, Plasmid diversity and phylogenetic consistency in the Lyme disease agent *Borrelia burgdorferi*. *BMC Genomics* **18**, 165 (2017).

8. T. N. Petersen, S. Brunak, G. von Heijne, H. Nielsen, SignalP 4.0: discriminating signal peptides from transmembrane regions. *Nature methods* **8**, 785-786 (2011).

9. K. Brangulis *et al.*, Structural characterization of CspZ, a complement regulator factor H and FHL-1 binding protein from *Borrelia burgdorferi*. *The FEBS journal* **281**, 2613-2622 (2014).

10. J. Chiu, P. E. March, R. Lee, D. Tillett, Site-directed, Ligase-Independent Mutagenesis (SLIM): a single-tube methodology approaching 100% efficiency in 4 h. *Nucleic acids research* **32**, e174 (2004).

11. U. Mueller *et al.*, Facilities for macromolecular crystallography at the Helmholtz-Zentrum Berlin. *J Synchrotron Radiat* **19**, 442-449 (2012).

12. M. D. Winn *et al.*, Overview of the CCP4 suite and current developments. *Acta crystallographica. Section D, Biological crystallography* **67**, 235-242 (2011).

13. P. R. Evans, An introduction to data reduction: space-group determination, scaling and intensity statistics. *Acta crystallographica. Section D, Biological crystallography* **67**, 282-292 (2011).

14. W. Kabsch, Xds. *Acta crystallographica. Section D, Biological crystallography* **66**, 125-132 (2010).

15. A. J. McCoy *et al.*, Phaser crystallographic software. *J Appl Crystallogr* **40**, 658-674 (2007).

16. K. Cowtan, The Buccaneer software for automated model building. 1. Tracing protein chains. *Acta crystallographica. Section D, Biological crystallography* **62**, 1002-1011 (2006).

17. P. Emsley, K. Cowtan, Coot: model-building tools for molecular graphics. *Acta crystallographica. Section D, Biological crystallography* **60**, 2126-2132 (2004).
18. G. N. Murshudov, A. A. Vagin, E. J. Dodson, Refinement of macromolecular structures by the maximum-likelihood method. *Acta crystallographica. Section D, Biological crystallography* **53**, 240-255 (1997).
19. J. Jumper *et al.*, Highly accurate protein structure prediction with AlphaFold. *Nature* **596**, 583-589 (2021).
20. S. M. Kelly, T. J. Jess, N. C. Price, How to study proteins by circular dichroism. *Biochimica et biophysica acta* **1751**, 119-139 (2005).
21. Y. P. Lin *et al.*, Fibronectin binds to and induces conformational change in a disordered region of leptospiral immunoglobulin-like protein B. *The Journal of biological chemistry* **284**, 23547-23557 (2009).
22. J. E. Purser, S. J. Norris, Correlation between plasmid content and infectivity in *Borrelia burgdorferi*. *Proceedings of the National Academy of Sciences of the United States of America* **97**, 13865-13870 (2000).
23. Y. P. Lin *et al.*, Strain-specific joint invasion and colonization by Lyme disease spirochetes is promoted by outer surface protein C. *PLoS pathogens* **16**, e1008516 (2020).
24. J. E. Purser *et al.*, A plasmid-encoded nicotinamidase (PncA) is essential for infectivity of *Borrelia burgdorferi* in a mammalian host. *Molecular microbiology* **48**, 753-764 (2003).
25. J. Feng, T. Wang, S. Zhang, W. Shi, Y. Zhang, An optimized SYBR Green I/PI assay for rapid viability assessment and antibiotic susceptibility testing for *Borrelia burgdorferi*. *PloS one* **9**, e111809 (2014).

26. Y. P. Lin *et al.*, Strain-specific variation of the decorin-binding adhesin DbpA influences the tissue tropism of the lyme disease spirochete. *PLoS pathogens* **10**, e1004238 (2014).
27. D. Drecktrah, D. S. Samuels, Genetic Manipulation of *Borrelia* Spp. *Current topics in microbiology and immunology* **415**, 113-140 (2018).
28. T. Hart, X. Yang, U. Pal, Y. P. Lin, Identification of Lyme borreliae proteins promoting vertebrate host blood-specific spirochete survival in *Ixodes scapularis* nymphs using artificial feeding chambers. *Ticks and tick-borne diseases* **9,** 1057-1063 (2018).
29. T. M. Hart *et al.*, Host tropism determination by convergent evolution of immunological evasion in the Lyme disease system. *PLoS pathogens* **17**, e1009801 (2021).
30. C. N. Takacs *et al.*, Polyploidy, regular patterning of genome copies, and unusual control of DNA partitioning in the Lyme disease spirochete. *Nature communications* **13**, 7173 (2022).
31. Y. Uno, T. Usui, Y. Fujimoto, T. Ito, T. Yamaguchi, Quantification of interferon, interleukin, and Toll-like receptor 7 mRNA in quail splenocytes using real-time PCR. *Poultry science* **91**, 2496-2501 (2012).
32. T. Petnicki-Ocwieja *et al.*, Nod2 suppresses *Borrelia burgdorferi* mediated murine Lyme arthritis and carditis through the induction of tolerance. *PloS one* **6**, e17414 (2011).
33. R. Rose, O. Golosova, D. Sukhomlinov, A. Tiunov, M. Prosperi, Flexible design of multiple metagenomics classification pipelines with UGENE. *Bioinformatics* **35**, 1963-1965 (2019).
34. H. Li, Aligning sequence reads, clone sequences and assembly contigs with BWA-MEM. *arXiv* **1303**, 3997 (2013).

35. F. Abascal, R. Zardoya, M. J. Telford, TranslatorX: multiple alignment of nucleotide sequences guided by amino acid translations. *Nucleic acids research* **38**, W7-13 (2010).

36. D. H. Huson, D. Bryant, Application of phylogenetic networks in evolutionary studies. *Mol Biol Evol* **23**, 254-267 (2006).

37. P. Villesen, FaBox: an online toolbox for fasta sequences. *Mol Ecol Notes* **7**, 965-968 (2007).

38. L. T. Nguyen, H. A. Schmidt, A. von Haeseler, B. Q. Minh, IQ-TREE: a fast and effective stochastic algorithm for estimating maximum-likelihood phylogenies. *Mol Biol Evol* **32**, 268-274 (2015).

39. S. Kalyaanamoorthy, B. Q. Minh, T. K. F. Wong, A. von Haeseler, L. S. Jermiin, ModelFinder: fast model selection for accurate phylogenetic estimates. *Nature methods* **14**, 587-589 (2017).

40. D. T. Hoang, O. Chernomor, A. von Haeseler, B. Q. Minh, L. S. Vinh, UFBoot2: Improving the Ultrafast Bootstrap Approximation. *Mol Biol Evol* **35**, 518-522 (2018).

41. I. Letunic, P. Bork, Interactive Tree Of Life (iTOL) v5: an online tool for phylogenetic tree display and annotation. *Nucleic acids research* **49**, W293-W296 (2021).

42. S. Kumar, G. Stecher, M. Li, C. Knyaz, K. Tamura, MEGA X: Molecular Evolutionary Genetics Analysis across Computing Platforms. *Mol Biol Evol* **35**, 1547-1549 (2018).

43. S. L. Kosakovsky Pond, D. Posada, M. B. Gravenor, C. H. Woelk, S. D. Frost, Automated phylogenetic detection of recombination using a genetic algorithm. *Mol Biol Evol* **23**, 1891-1901 (2006).

748 44. B. Murrell *et al.*, Gene-wide identification of episodic selection. *Mol Biol Evol* **32**, 1365-
749 1371 (2015).
750 45. S. R. Wisotsky, S. L. Kosakovsky Pond, S. D. Shank, S. V. Muse, Synonymous Site-to-
751 Site Substitution Rate Variation Dramatically Inflates False Positive Rates of Selection
752 Analyses: Ignore at Your Own Peril. *Mol Biol Evol* **37**, 2430-2439 (2020).
753 46. B. Murrell *et al.*, FUBAR: a fast, unconstrained bayesian approximation for inferring
754 selection. *Mol Biol Evol* **30**, 1196-1205 (2013).
755 47. S. L. Kosakovsky Pond, S. D. Frost, Not so different after all: a comparison of methods for
756 detecting amino acid sites under selection. *Mol Biol Evol* **22**, 1208-1222 (2005).
757 48. B. Murrell *et al.*, Detecting individual sites subject to episodic diversifying selection. *PLoS*
758 *genetics* **8**, e1002764 (2012).
759 49. S. Weaver *et al.*, Datamonkey 2.0: A Modern Web Application for Characterizing
760 Selective and Other Evolutionary Processes. *Mol Biol Evol* **35**, 773-777 (2018).
761 50. S. Q. Le, O. Gascuel, An improved general amino acid replacement matrix. *Mol Biol Evol*
762 **25**, 1307-1320 (2008).
763 51. C. M. Ross, G. Foley, M. Boden, E. M. J. Gillam, Using the Evolutionary History of
764 Proteins to Engineer Insertion-Deletion Mutants from Robust, Ancestral Templates Using
765 Graphical Representation of Ancestral Sequence Predictions (GRASP). *Methods in*
766 *molecular biology* **2397**, 85-110 (2022).
767 52. M. Musil *et al.*, FireProtASR: A Web Server for Fully Automated Ancestral Sequence
768 Reconstruction. *Brief Bioinform* **22** (2021).

53. M. A. Suchard *et al.*, Bayesian phylogenetic and phylodynamic data integration using BEAST 1.10. *Virus Evol* **4**, vey016 (2018).

54. M. Hasegawa, H. Kishino, T. Yano, Dating of the human-ape splitting by a molecular clock of mitochondrial DNA. *J Mol Evol* **22**, 160-174 (1985).

55. Z. Yang, Maximum likelihood phylogenetic estimation from DNA sequences with variable rates over sites: approximate methods. *J Mol Evol* **39**, 306-314 (1994).

56. K. S. Walter, G. Carpi, A. Caccone, M. A. Diuk-Wasser, Genomic insights into the ancient spread of Lyme disease across North America. *Nat Ecol Evol* **1**, 1569-1576 (2017).

57. X. Robert, P. Gouet, Deciphering key features in protein structures with the new ENDscript server. *Nucleic acids research* **42**, W320-324 (2014).

58. A. M. Waterhouse, J. B. Procter, D. M. Martin, M. Clamp, G. J. Barton, Jalview Version 2--a multiple sequence alignment editor and analysis workbench. *Bioinformatics* **25**, 1189-1191 (2009).

59. Y. K. Benjamini, A. M. Yekutieli, D. , Adaptive linear step-up procedures that control the false discovery rate. *Biometrika* **93**, 491-507 (2006).

60. A. L. Marcinkiewicz *et al.*, Eliminating Factor H-Binding Activity of *Borrelia burgdorferi* CspZ Combined with Virus-Like Particle Conjugation Enhances Its Efficacy as a Lyme Disease Vaccine. *Frontiers in immunology* **9**, 181 (2018).

61. T. Hallstrom *et al.*, CspA from *Borrelia burgdorferi* inhibits the terminal complement pathway. *mBio* **4** (2013).

62. A. F. Elias *et al.*, Clonal polymorphism of *Borrelia burgdorferi* strain B31 MI: implications for mutagenesis in an infectious strain background. *Infection and immunity* **70**, 2139-2150 (2002).

63. A. S. Coleman *et al.*, *Borrelia burgdorferi* complement regulator-acquiring surface protein 2 does not contribute to complement resistance or host infectivity. *PloS one* **3**, 3010e (2008).

64. V. M. Benoit, J. R. Fischer, Y. P. Lin, N. Parveen, J. M. Leong, Allelic variation of the Lyme disease spirochete adhesin DbpA influences spirochetal binding to decorin, dermatan sulfate, and mammalian cells. *Infection and immunity* **79**, 3501-3509 (2011).

65. K. L. Frank, S. F. Bundle, M. E. Kresge, C. H. Eggers, D. S. Samuels, *aadA* confers streptomycin resistance in *Borrelia burgdorferi*. *Journal of bacteriology* **185**, 6723-6727 (2003).